AGU PUBLICATIONS

Geochemistry, Geophysics, Geosystems

RESEARCH ARTICLE
10.1002/2015GC005861

Key Points:
- Ferromanganese and phosphorite mineral deposits discovered on Galicia Bank
- Paragenesis are controlled by hydrogenous, diagenetic, and hydrothermal processes
- Cenozoic tectonism and paleoceanography are recorded on the mineralizations

Supporting Information:
- Supporting Information S1
- Figure S1
- Figure S2
- Figure S3

Correspondence to:
F. J. González,
fj.gonzalez@igme.es

Citation:
González, F. J., L. Somoza, J. R. Hein, T. Medialdea, R. León, V. Urgorri, J. Reyes, and J. A. Martín-Rubí (2016), Phosphorites, Co-rich Mn nodules, and Fe-Mn crusts from Galicia Bank, NE Atlantic: Reflections of Cenozoic tectonics and paleoceanography, *Geochem. Geophys. Geosyst.*, *17*, 346–374, doi:10.1002/2015GC005861.

Received 17 APR 2015
Accepted 19 JAN 2016
Accepted article online 29 JAN 2016
Published online 10 FEB 2016

Phosphorites, Co-rich Mn nodules, and Fe-Mn crusts from Galicia Bank, NE Atlantic: Reflections of Cenozoic tectonics and paleoceanography

Francisco Javier González[1], Luis Somoza[1], James R. Hein[2], Teresa Medialdea[1], Ricardo León[1], Victoriano Urgorri[3], Jesús Reyes[1], and Juan Antonio Martín-Rubí[1]

[1]Geological Survey of Spain, IGME, Madrid, Spain, [2]U. S. Geological Survey, Pacific Coastal and Marine Science Center, Santa Cruz, California, USA, [3]Estación de Bioloxía Mariña da Graña, Universidade de Santiago de Compostela, Ferrol, Spain

Abstract A wide variety of marine mineral deposits were recovered from 750 to 1400 m water depths on Galicia Bank, Iberian margin. Mineral deposits include: (1) carbonate fluorapatite phosphorite slabs and nodules that replaced limestone and preserved original protolith fabric. (2) Ferromanganese vernadite crusts with high Mn and Fe (Mn/Fe = 1) contents, and thick stratabound layers consisting mainly of Mn (up to 27% MnO) and Fe (15% Fe_2O_3), which impregnated and replaced the phosphorite. (3) Co-rich Mn nodules are composed of romanechite and todorokite laminae. Mn-rich layers (up to 58% MnO) contain up to 1.8% Co. (4) Goethite nodules with Fe up to 67% Fe_2O_3 have low Mn and trace metals. We interpret this mineralization paragenesis to be related to major changes in oceanographic and tectonic regimes. Three phosphatization generations formed hardgrounds dated by $^{87}Sr/^{86}Sr$ isotopes as late Oligocene, early Miocene, and latest early Miocene. During the latest early Miocene, the hardground was fractured and breached due to regional intraplate tectonism, which was coeval with a widespread regional erosional unconformity. The stratabound layers and Co-rich manganese nodules were derived from low-temperature geothermally driven hydrothermal fluids, with fluid conduits along reactivated faults. During middle and late Miocene, the introduction of vigorous deep water flow from the Arctic generated growth of hydrogenetic ferromanganese crusts. Finally, growth of diagenetic Fe-rich nodules (late Pliocene) was promoted by the introduction of hypersaline Mediterranean Outflow Water into the Atlantic Ocean.

1. Introduction

Marine mineral deposits are metal-rich chemical sediments that are archives for paleoceanographic proxies and are potential mineral resources. Several main mineral deposits are found on the seafloor: Fe-Mn crusts and nodules, phosphorites, and seafloor massive sulphides [e.g., *Rona*, 2008; *Hein et al*., 2013]. Traditionally, marine precipitates are defined as purely hydrogenetic when all constituents are derived from cold seawater, as diagenetic when all constituents are derived from cold sediment pore water, and as hydrothermal when precipitation occurs in the vicinity of hydrothermal vent sites from fluids with temperatures higher than ambient bottom waters [*Bau et al*., 2014]. Hydrogenetic Fe-Mn crusts occur throughout the global ocean on seamounts, ridges, and plateaus where currents have kept the rocks free of sediment for millions of years [e.g., *Aplin and Cronan*, 1985; *De Carlo et al*., 1987; *Pichocki and Hoffert*, 1987; *Usui and Someya*, 1997; *Hein et al*., 2000]. Some ferromanganese (Fe-Mn) crusts and nodules exhibit a mixed origin, primarily either hydrothermal-hydrogenetic or hydrogenetic-diagenetic [e.g., *Baturin and Drovetsova*, 2014]. In discussions of Cenozoic marine Fe-Mn oxyhydroxide precipitates, it is common to distinguish between hydrothermal deposits, hydrogenetic crusts, and diagenetic nodules [*Bau et al*., 2014].

In many places, marine phosphorite is accompanied by Fe-Mn mineralization [*Baturin*, 1982; *Hein et al*., 1985; *Rao and Burnett*, 1992; *Benninger and Hein*, 2000]. Some thick Fe-Mn crusts also contain carbonate fluorapatite (CFA), which was incorporated into the crusts during specific periods prior to middle Miocene [*Baturin*, 1982; *Hein et al*., 1985; *Rao and Burnett*, 1992; *Benninger and Hein*, 2000]. This type of mineralization seems to have occurred during two main Cenozoic episodes of phosphatization: the Eocene-Oligocene (39–

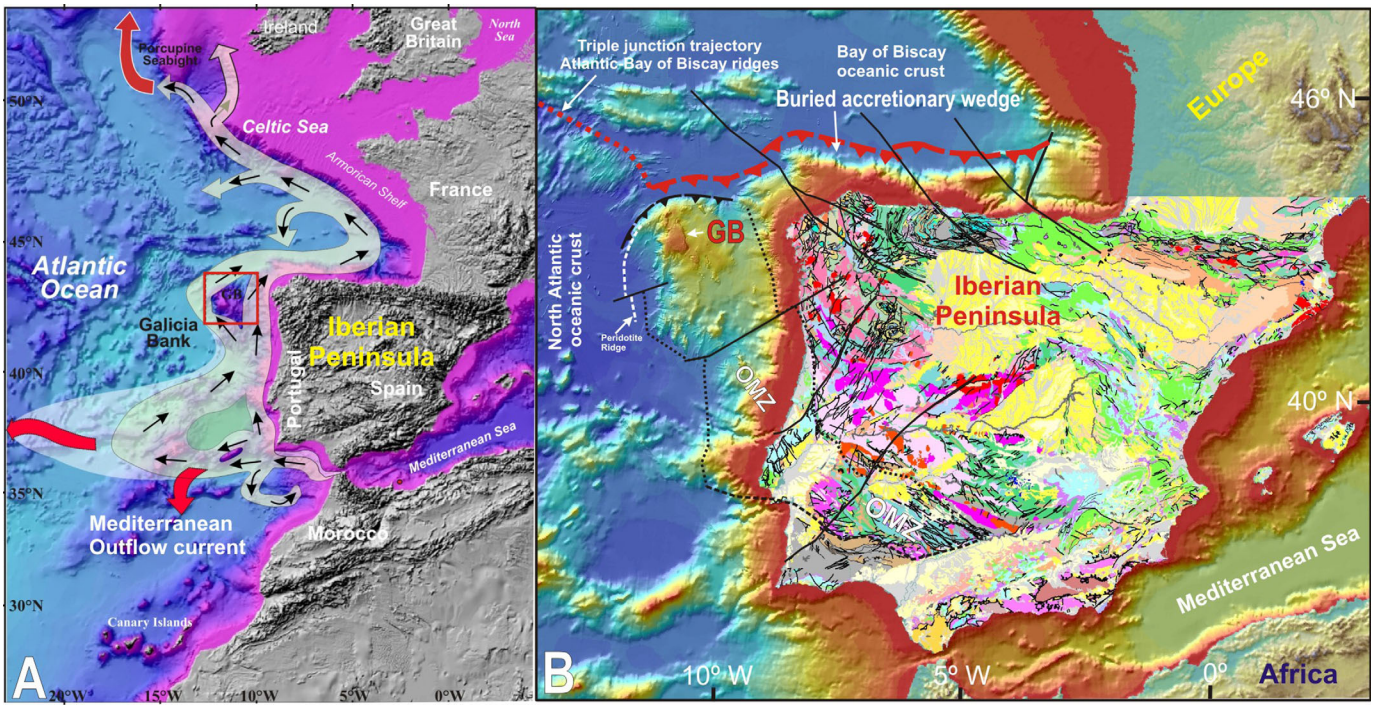

Figure 1. Geological setting of Galicia Bank region. (a) Location of Galicia Bank and pathways of the Mediterranean Outflow undercurrent along the eastern Atlantic margin (modified from *Somoza et al*. [2014]). (b) Geological setting of the Iberian Peninsula from the IGME Geological Map at scale 1:1.000.000 [*Rodríguez Fernández et al*., 2016; *Capdevila and Mougenot*, 1988]. OMZ = Ossa-Morena Zone is the onshore geological zone of the Variscan Iberian Massif that seems to continued offshore into the Galicia Bank (GB) offset by left-lateral strike slips faults. The buried accretionary wedge of the North Iberian margin offset by strike-slip faults is also depicted. Note that Galicia Bank is bounded to the north by the Bay of Biscay oceanic crust and to the west by the North Atlantic, which are separated by the trajectory of the fossil triple junction between the north Atlantic and the Bay of Biscay spreading ridges (bathymetry from *GEBCO* [2003]).

34 Ma) and Oligocene-Miocene (27–21 Ma) with potentially other minor phosphogenic events, especially the middle Miocene, about 15 Ma ago [*Hein et al*., 1993].

Phosphorite deposits are widespread on the seafloor of continental shelves and slopes along the western continental margins of both the Pacific and Atlantic Oceans. These deposits are related to strong upwelling, such as along the Pacific Peru-Chile margin and the Atlantic Morocco, Senegal, and Namibia margins [e.g., *Tooms and Summerhayes*, 1968; *Burnett*, 1977; *Pascal et al*., 1989; *Föllmi*, 1996]. Phosphogenesis driven by sulphur bacteria has been recently described in different upwelling areas such as the Namibian shelf [e.g., *Schulz and Schulz*, 2005; *Arning et al*., 2008]. Phosphorite also occurs on seamounts and plateaus, such as the Blake Plateau off the southeastern U.S. and on carbonate islands or atolls that occur in the western and central Pacific or eastern equatorial Atlantic [e.g., *Manheim et al*., 1980; *Baturin*, 1982; *Hein et al*., 1993; *Benninger and Hein*, 2000; *Jones et al*., 2002].

Research on phosphorite and Fe-Mn deposits have traditionally had two main purposes: (1) their economic importance as potential sources of phosphate for agriculture and metals, rare earth elements plus yttrium (REY), among others, required for high-tech applications [*Hein et al*., 2013], and (2) their potential as archives for the study of paleoceanographic events [*Baturin*, 1988; *Hein et al*., 1993; *Rona*, 2008; *Hein et al*., 2010; *Baturin and Dubinchuk*, 2011]. Phosphorite and Fe-Mn nodule and crust studies from continental-margin deposits and associated seamounts and banks have been the focus of numerous studies since the 1950s, however, few of those studies dealt with the mineral paragenesis of phosphatization and Fe-Mn mineralization, and their relationships to paleoceanographic events [e.g., *Hein and Morgan*, 1999; *Benninger and Hein*, 2000]. Studies of phosphatization in low-organic carbon settings, with moderate to low primary productivity [*Benninger and Hein*, 2000] are also not common.

This paper presents the first studies of phosphorite hardgrounds and a suite of Fe-Mn oxyhydroxide deposits (nodules and crusts) discovered in the Galicia Bank region (northwest Iberian margin, NE Atlantic). We present results for a complete suite of mineral deposit types: (1) phosphorite slabs and nodules, (2) Fe-Mn

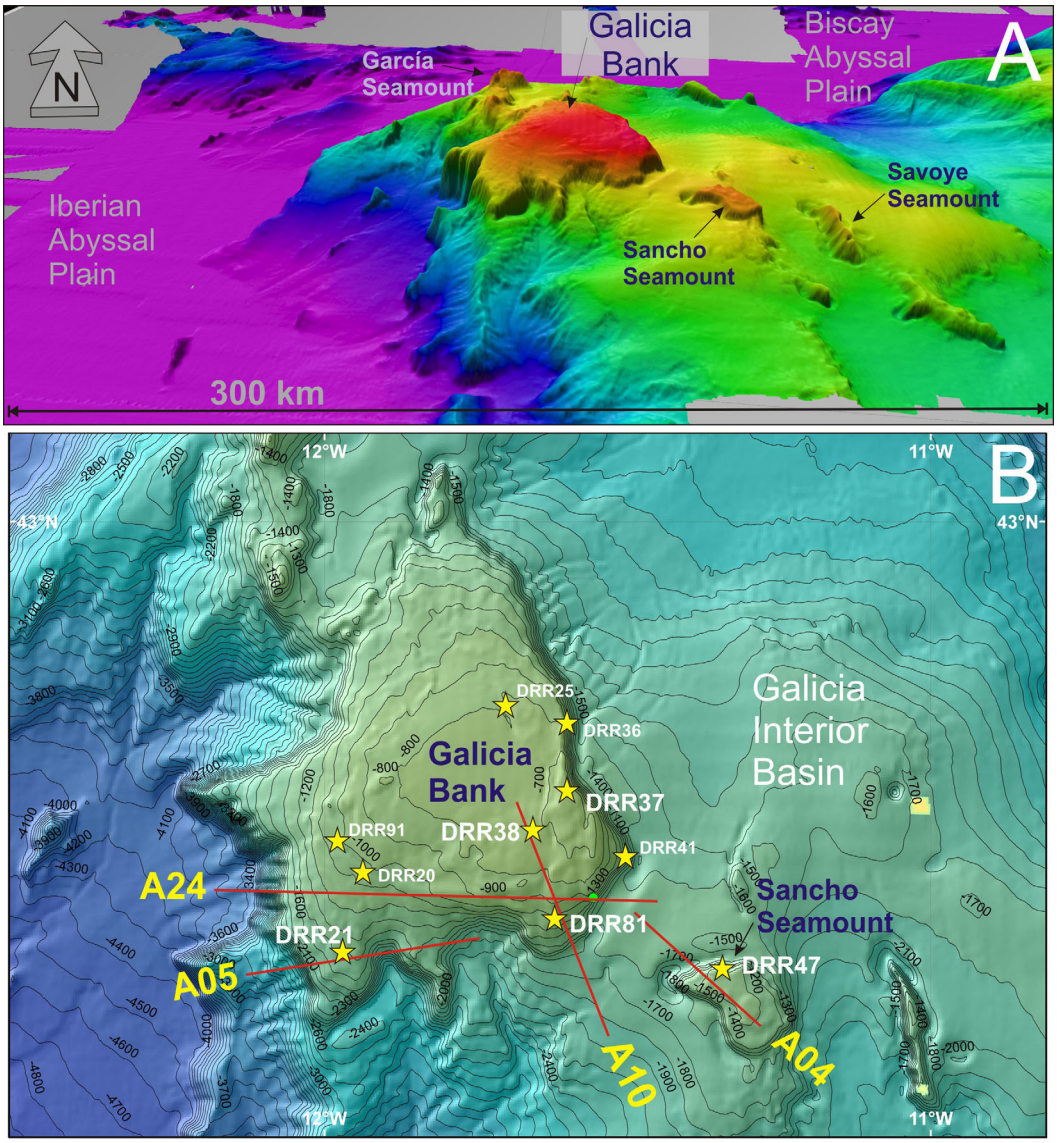

Dredge station	Water depth (m)	Geomorphic feature	Area	Morphological characterization	Types of mineral deposits
DRR21	1490-1380	Galicia Bank	SW margin	mound structures	**I, III**
DRR36	1555-760	Galicia Bank	E slope	Fault scarps	**I**
DRR37	1323-630	Galicia Bank	E slope to summit	Hummocky topography, sediment waves and furrows	**IV**
DRR38	760-721	Galicia Bank	E summit		**IV**, II
DRR47	1650-1165	Sancho Seamount	N slope to summit	Coral patches	**I, II**
DRR81	1540-830	Galicia Bank	SE margin	High scarps	**I, II**, III

Figure 2. (top) Three-dimensional multibeam bathymetric image (Simrad EM12-120S), Fledermaus visualization of the seabed structure map in the study area. Viewing direction is from the South. (bottom) Data sets used, including dredge hauls (stars), multichannel seismic reflection lines (red lines), and simplified bathymetry. Table below: data set of the most relevant morphological characteristics of the dredge stations selected for this study.

crusts and stratabound deposits, (3) Co-rich Mn nodules, and (4) Fe-rich nodules, based on detailed mineralogy, petrography, and chemical analyses. Furthermore, we present geophysical data including multibeam bathymetry echo sounder (MBES) mosaics and multichannel high-resolution seismic (MHRS) profiles of the areas where the hardgrounds, crusts, and nodules were collected. The MHRS profiles allow us to place these deposits into the framework of Cenozoic seismostratigraphic Units and their ages. Ages of phosphatization were estimated using strontium isotope stratigraphy and micropaleontology. Finally, we propose genetic

models for the different types of mineral deposits and relate those to key paleoceanographic and tectonic events that occurred in the North Atlantic since the late Oligocene. These events influenced the global Thermohaline Circulation (THC) of the North Atlantic Ocean.

2. Geological and Hydrographic Framework

2.1. Geological Setting and Bank Morphology

Galicia Bank is situated along the northwest Iberia margin 200 km west of Galicia (Figure 1), between 42°15′N and 43°N and 11°30′W and 12°15′W at water depths of 700–1800 m. The northwest Iberia margin is wide (up 350 km) and hosts several seamounts (e.g., Sancho, García, and Savoye seamounts, Figure 2) [*Ercilla et al*., 2011]. Galicia Bank, with an area of 2117 km^2, is the main structural high of the northwest Iberian margin, emerging from a depth of 3800–620 m [e.g., *Vanney et al*., 1979]. The bank is a horst bounded to the east by a NW-SE scarp of 800 m relief, to the south by NE-SW normal faults that produced a scarp of 600 m relief, to the west by a N-S normal fault forming a scarp 2000 m high, and to the north by a NE–SW normal fault [*Ercilla et al*., 2009, 2011; *Vázquez et al*., 2009a]. Galicia Bank and other seamounts such as Vasco de Gama, Porto, and Vigo are Mesozoic structural highs reactivated and uplifted during Cenozoic Pyrenean tectonics, related to the Iberia-Eurasia convergence during the Paleogene.

Based on stratigraphy determined from dredged samples and micropaleontological studies of the seamounts and banks [*Groupe Galicia*, 1979], it appears that during the Late Cretaceous, the western Iberian margin had already undergone strong subsidence, except for Galicia Bank, which probably was a slightly submerged shoal. Furthermore, micropaleontological data indicate that Galicia Bank continued to be in the neritic zone at least until the beginning of the Cenozoic [*Dupeuble et al*., 1976].

Several morpho-tectonic structures testify to tectonic reactivation of Galicia Bank during the Cenozoic [*Vázquez et al*., 2008]: (1) faults inherited from the Cretaceous propagating rift (reactivated and non-reactivated), including reactivated normal (N-S, NW-SE) and strike-slip (NE-SW) faults, and (2) Structures resulting from episodes of compression during the Paleogene to late Miocene and late Miocene to present, including (a) late Miocene-Quaternary normal faults, (b) folds, flexures, and (c) reverse faults (NE-SW to ENE-SWS). The reactivation phase along the NW flank produced 3500 m relief parallel to reverse faults and normal to the main convergence.

2.2. Present-Day Oceanographic Setting

Several water masses off the northwest Iberian margin affect Galicia Bank [e.g., *Rios et al*., 1992; *Bode et al*., 2002]. Waters above 500 m are dominated by eastern North Atlantic Central Water (ENACW), of which two subtypes were identified based on origin and temperature and salinity characteristics [*McCartney and Talley*, 1982; *Pollard and Pu*, 1985]. The subtropical subtype (ENACWt) ranges from 12.2 to 18.5°C and from 35.66 to 36.75‰ salinity and its origin is located in a front near the Azores [*Fiúza*, 1984]. The subpolar type (ENACWp) formed around 46°N with water between 4 and 12°C and 34.96–35.66‰ salinity [*Harvey*, 1982]. Below the salinity minimum near 500 m depth, ENACW gradually mixes with intermediate Mediterranean water, which reaches peak salinity at approximately 1000 m depth. This water mass is characterized by two cores located at 800 and 1200 m depths showing increased salinity [*Ambar and Howe*, 1979; *Iorga and Lozier*, 1999; *Garcia-Lafuente et al*., 2008], and moves as a contour current reaching velocities of 5–10 cm/s [*Daniault et al*., 1994; *Iorga and Lozier*, 1999]. Deep water masses below 1500 m include the Labrador Sea Water (LSW), North Atlantic Deep Water (NADW), and Lower Deep Water (LDW). These water masses result from the mixing of different water masses depending on density. Below the LSW, and originating from the mixing of southward moving water masses formed in the Arctic Ocean, the NADW reaches to the Galicia margin moving northward. The core is located along this margin approximately between 2500 and 3000 m depth [*Saunders*, 1986]. Below the NADW (about 4000 m water depth), the LDW flows northward [*Paillet and Mercier*, 1997; *Van Aken*, 2000].

3. Data and Methods

Detailed information about the geophysical, sampling, mineralogical, and geochemical techniques can be found in the supporting information.

3.1. Bathymetry and Seismic Reflection Data

The geophysical data sets used here were acquired within the framework of the ERGAP project during two cruises (ERGAP-1 and ERGAP-2) carried out in 2007 aboard the R/V *LÁtalante*. The geophysical data obtained during these cruises included multichannel high-resolution seismic (MHRS) and multibeam bathymetry echo sounder (MBES) records, which allowed us to explore Galicia Bank in detailed.

3.2. Sample Analyses Techniques

Samples were collected aboard the R/V *Sarmiento de Gamboa* in 2009 via dredging at water depths from 1200 to 700 m during cruise DIVA-ARTABRIA II. Previous MBES backscatter data and MHRS profiles indicated the presence of deposits sampled: mounds and surfaces of high, −12 to −20 dB, acoustic backscatter, vertical fluid emission structures, and high-amplitude and reflectivity reflectors.

A suite of 16 representative mineralization samples from stations DRR21, DRR37, DRR38, DRR47, and DRR81 were selected for this work (Tables (1–3)). Mineralogical analyses were carried out using X-ray diffraction (XRD), and optical and electron microscopy (SEM and EPMA). The abundance of major, minor, and trace elements, as well as REY was determined by spectrometric techniques (XRF, ICP-MS, ICP-AES, and AAS), and Thermal Ionization Mass Spectrometry (TIMS) was used for Sr and Nd isotopic determinations.

4. Results

Four types of mineral deposits collected from the Galicia Bank region were identified: Type I: phosphorite slabs and nodules; Type II: Fe-Mn crusts and stratabound layers; Type III: Co-rich Mn nodules; and Type IV: Fe-rich nodules. These different types of mineralization are distributed in different physiographic environments over Galicia Bank and Sancho seamount (Figure 2).

4.1. Seismostratigraphic Analysis: Major Discontinuities, Hardgrounds, and Sample Sites

Three seismostratigraphic Units (U1, U2, and U3) are identified for Galicia Bank and Sancho seamount, separated by two main discontinuities (D1 and D2) (Figures 3 and 4 and supporting information Figures S1 and S2). The main unconformity identified along the bank is D1, characterized by high-amplitude reflectors that constituted a ramp-type seafloor over most of the bank. In places, the high-reflectivity character of the D1 unconformity masks the underlying Units on Galicia Bank, that we call U1 Unit (supporting information Figure S2). Samples of large phosphorite slabs (<1 m) collected at stations DRR81 and DRR21 are related to this D1 unconformity, which forms the morphological margin of Galicia Bank (Figure 3). D1 is also identified at the summit of Sancho seamount overlying the lowermost sedimentary Unit U1. Samples from station DRR47 along the top of this seamount also yielded large phosphorite slabs with Mn replacement along the top and underside surfaces (Figure 5).

The D1 unconformity is overlain by Unit U2 along the western side of Galicia Bank. Unit U2 is composed of a westward up-slope migrating drift developed from 1570 to 1125 m water depths (Figure 3 and supporting information Figure S2). Unit U2 is also well developed along the foot of southern Galicia Bank and in the passage between Sancho seamount and Galicia Bank overlying a faulted and deformed D1 reflector (Figure 3 and supporting information Figure S1). The top of Unit U2 is a highly erosive unconformity, D2, seen in the present morphology as a moat (Figure 3 and supporting information Figure S2).

Seismic chimneys (SC in Figure 4) composed of semitransparent acoustic facies interrupt the sequence of reflectors of Unit U1 and partially of Unit U2. Furthermore, these seismic chimneys breach the D1 unconformity and form mounds with internally chaotic acoustic facies that extend laterally overlapping this unconformity (Figures 3 and 4). Phosphorite pebbles (fragmented phosphorite), Co-rich Mn nodules, and Mn-impregnations of phosphorite slabs occur at stations DRR81 (Figure 3) and DRR47 and DRR21 (Figure 4) and are related to sites where breaching of horizon D1 occurred at the base of Unit U2.

Unit U3 occurs predominantly along the summit of Galicia Bank and is deposited on erosional unconformity D2. Unit U3 is composed of fossil and living deep water coral forming along-slope oriented mounds and ridges and is intercalated with up-slope migrating sediment drifts at water depths from 1125 to 826 m, which are related to the Mediterranean Outflow Water [*Somoza et al.*, 2014]. Fe-rich nodules recovered at stations DRR37 and DRR38 are related to Unit U3 (Figure 3).

Table 1. Chemical Composition of Selected Phosphorite Samples

	(Type I) Phosphorite Slabs and Nodules						
	DRR47-1A	DRR81-5B	DRR47-2	DRR81-3	DRR81-4	DRR38-2	
	Phosphorite	Phosphorite	Phosphorite Pebbles	Phosphorite	Phosphorite	Phosphorite Nodule	Av. Shale[a,b]
Al_2O_3 (wt %)	0.72	1.05	2.35	1.23	1.86	1.14	15.12
SiO_2	2.34	2.27	3.35	3.23	4.82	1.38	59.96
P_2O_5	22.3	32.6	25.8	22.1	30.6	31.1	0.16
K_2O	0.15	0.25	0.46	0.35	0.50	0.16	3.21
Na_2O	0.62	0.87	0.92	0.68	0.89	0.90	1.3
CaO	48.7	45.2	32.6	46.1	42.5	37.7	3.1
MgO	0.68	0.86	1.92	0.96	1.12	0.95	2.5
TiO_2	0.02	0.18	0.23	0.04	0.42	0.24	0.77
Fe_2O_3	0.28	1.72	8.18	2.83	3.27	8.80	6.75
MnO	0.82	1.1	10.3	0.70	1.79	5.35	0.11
TOC		0.38	0.42	0.36	0.31	0.24	
S	0.30	0.50	0.39	0.37	0.56	0.04	0.24
F	0.57	2.03	1.69	1.42	2.08	2.43	0.074
LOI	23.4	13.8	13.0	21.8	12.1	12.3	
CaO/P_2O_5	2.18	1.39	1.26	2.09	1.39	1.21	19.38
F/P_2O_5	0.03	0.06	0.07	0.06	0.07	0.08	0.46
Ag (μg/g)	<DL	<DL	<DL	<DL	<DL	<DL	0.07
As	8	38	147	50	51	177	13
Ba	71	103	1588	247	123	941	580
B	191	187	256	199	291	359	100
Co	36	113	1420	142	354	1322	19
Cr	2	6	13	31	5	4	90
Cu	52	92	845	57	121	131	45
Li	5	9	56	7	11	6	66
Mo	8	25	90	9	33	71	2.6
Nb	3	8	13	4	6	23	11
Ni	371	449	3798	257	552	734	68
Pb	13	53	572	23	128	911	20
Rb	<DL	4	12	8	17	2	140
Sb	<DL	5	9	4	2	18	1.5
Sc	3	13	10	10	15	7	13
Se	4	2	3	1	<DL	21	0.6
Sr	785	865	989	897	936	1750	300
Te			20				0.08
Th	0.75	2.7	7.7	2.3	3.6	6.8	12
Tl	<DL	1	40	<DL	5	<DL	1.2
U	6.1	6.4	6.5	6.3	5.3	8.3	3.7
V	16	61	272	64	89	282	130
W	4	11	23	4	7	18	1.8
Zn	54	76	478	203	118	208	95
U/Th	8.13	2.41	0.85	2.80	1.47	1.22	0.31
La	17.3	134	368	125	216	275	92
Ce	7.18	35.8	278	28.8	68.5	920	59
Pr	2.23	19.1	50.6	19.7	24.6	32.7	5.6
Nd	8.99	84.2	215	84.9	105	131	24
Sm	1.66	16.8	40.2	16.5	19.9	23.8	6.4
Eu	0.41	4.51	10.4	4.14	5.34	6.14	1.0
Gd	2.05	24.3	57.2	21.5	30.2	37.8	6.4
Tb	0.31	3.78	8.01	3.24	4.48	4.96	1.0
Dy	2.11	25.6	51.5	20.8	30.6	32.4	4.6
Y	27	306	664	178	455	411	26
Ho	0.55	6.17	12.2	4.84	7.61	8.05	1.2
Er	1.94	19.3	36.6	14.6	23.9	25.4	2.5
Tm	0.3	2.68	4.74	2.01	3.29	3.51	0.2
Yb	0.19	17.2	28.4	12.9	21.3	22.1	2.6
Lu	0.4	2.91	4.67	2.11	3.64	3.74	2.8
%HREY	49	59	48	49	57	29	20
Ce*	−0.62	−0.83	−0.37	−0.90	−0.73	+0.3	

[a]Turekian and Wedepohl [1961].
[b]*Baturin* [1988].

Table 2. Chemical Composition of Selected Fe-Mn Oxide Samples

	(Type II) Fe-Mn Deposits		(Type III) Co-Rich Mn Nodules			(Type IV) Fe-Rich Nodules		
	DRR47-1B Stratabound	DRR81-5A Fe-Mn crust	DRR81-1	DRR21-1	DRR21-2	DRR38-5	DRR37-1	Av. Nodules[a]
Al_2O_3 (wt %)	4.06	4.94	1.21	1.51	1.00	1.90	2.66	5.1
SiO_2	5.42	1.49	0.97	3.12	2.94	5.23	6.32	16.5
P_2O_5	10.8	1.17	0.42	0.17	0.15	1.03	0.77	0.85
K_2O	0.60	0.25	0.86	1.17	0.85	0.27	0.40	0.88
Na_2O	1.04	1.89	1.06	1.24	0.83	0.37	0.37	2.66
CaO	14.0	3.32	16.2	4.25	14.5	0.93	0.57	3.12
MgO	4.52	5.87	2.90	2.83	1.23	3.68	3.38	2.61
TiO_2	0.28	0.93	0.07	0.22	0.18	0.12	0.14	1.15
Fe_2O_3	15.4	23.8	0.45	0.42	1.33	67.4	64.6	17.8
MnO	23.3	27.6	49.9	58.2	54.0	2.08	4.96	24.0
LOI	19.0	26.8	22.2	19.3	18.3	17.0	15.8	-
Mn/Fe	1.7	1.3	123	153	45	0.03	0.09	1.35
Ag (μg/g)	<LD	<LD	<LD	<LD	<LD	<LD	<LD	0.09
As	258	500	48	64	46	274	156	140
Ba	2074	1042	25300	31900	58900	55	165	2300
B	337	362	183	205	199	440	519	300
Co	3663	8510	18005	14844	6482	94	86	2700
Cr	17	16	3	130	13	23	15	70
Cu	1539	783	1550	2201	1684	7	16	4500
Li	84	45	9	20	11	8	26	80
Mo	335	387	220	244	236	37	37	380
Nb	22	71	11	11	55	4	<LD	70
Ni	8627	6542	2328	2063	985	54	96	6600
Pb	745	2842	2580	6240	372	21	20	930
Rb	16	4	4	16	12	15	20	17
S	3124	5419	1116	1931	1633	675	532	4700
Sb	23	33	8	12	26	<LD	<LD	50
Sc	14	9	2	2	3	9	3	10
Se	<LD	<LD	<LD	<LD	<LD	<LD	<LD	0.6
Sr	737	1068	1730	1890	4288	78	109	830
Te			12	14	8		1	10
Th	8.8	25	1.7	6.0	1.4	1.6	1.5	30
Tl	15	81	122	116	42	<LD	7	150
U	6.8	12	2.7	4.1	3.0	3.4	1.7	5
V	700	983	1740	2550	3300	362	267	500
W	55	97	438	622	479	5	3	100
Zn	961	687	169	381	203	81	86	1200
La	146	114	23.5	32.1	21.3	9.69	5.03	157
Ce	217	1154	86.5	314	70.6	20.2	10.3	530
Pr	26	22.9	4.27	5.4	3.53	2.29	1.2	36
Nd	113	91.4	18.3	20.8	14.3	9.57	4.7	158
Sm	23.2	20.8	4.07	4.5	3.39	2.2	1.03	35
Eu	6.09	5.22	3.45	4.11	6.41	0.59	0.27	9
Gd	31.8	27.8	5.75	7.41	4.74	2.64	1.14	32
Tb	4.64	4.18	0.77	0.85	0.54	0.41	0.17	5.4
Dy	29.9	26.6	4.7	4.97	3.15	2.53	0.94	31
Y	245	130	26	20	13	13	5	150
Ho	6.86	5.8	1	1.04	0.62	0.52	0.19	7
Er	20.5	18	2.85	3.03	1.7	1.56	0.55	18
Tm	2.81	2.67	0.39	0.44	0.24	0.23	0.07	2.3
Yb	17.9	17.5	2.52	3.04	1.75	1.63	0.46	20
Lu	2.88	2.7	0.37	0.44	0.24	0.27	0.07	1.8
%HREY	41	15	26	11	23	35	29	21
Ce*	−0.11	0.72	0.28	0.73	0.26	0.00	0.00	
Y/Ho	36	22	26	13	32	25	26	21
Ce_{SN}/Ce_{SN*}	0.80	5.18	1.97	5.41	1.84	0.99	0.96	
Y_{SN}/Ho_{SN}	1.32	0.83	0.97	0.71	0.80	0.95	0.96	

[a]Global mean of oceanic Mn nodules from *Baturin* [1988].

Table 3. Sr and Nd Isotopic Compositions, Ages, and Descriptions of Galicia Bank Mineralization[a]

Sample Number	Type	Fossil Age	$^{87}Sr/^{86}Sr$	Sr Age (Ma)	$^{143}Nd/^{144}Nd$	$\varepsilon_{Nd(0)}$	Description
DRR47-1A	CFA	early Miocene	0.713355		0.512089	−10.71	Hydrothermal(?) CFA-replaced white limestone with foraminifera
DRR47-1A$_c$	Carbonate fraction	early Miocene	0.708611	17.7 ± 0.9			Analysis for Sr isotopes on 2.5 N HCl-leached sample
DRR81-3	CFA		0.714808		0.512149	−9.54	Hydrothermal(?) CFA-replaced pale brown limestone
DRR81-3$_c$	Carbonate fraction		0.708386	21 ± 0.6			Analysis for Sr isotopes on 2.5 N HCl-leached sample
DRR81-4	CFA		0.713657				Hydrothermal(?) CFA-replaced reddish limestone
DRR81-4$_c$	Carbonate fraction		0.708160	24.85 ± 0.9			Analysis for Sr isotopes on 2.5 N HCl-leached sample
DRR81-5B	CFA	early Miocene	0.712385		0.512146	−9.60	Hydrothermal(?) CFA-replaced reddish foraminiferal limestone
DRR47-2	Bulk	early Miocene?	0.708576	18.15 ± 0.4	0.512198	−8.58	CFA in phosphorite replaced by Mn oxide at a later stage
DRR37-1	Bulk		0.710637		0.512184	−8.86	Fe-rich nodule
DRR21-1	Bulk	Miocene?	0.708239	23.25 ± 0.6	0.512169	−9.15	Hydrothermal(?) Co-rich Mn nodule

[a]The Sr-isotope seawater curve of *McArthur and Howarth* [2004] was used. The ages of phosphatization could not be determined from Sr isotopes because the ratios were altered by interaction with hydrothermal fluids; the phosphatization was early diagenetic, so the depositional ages approximate the phosphatization ages.

4.2. Structure, Petrography, and Mineralogy

4.2.1. Phosphorite Slabs and Nodules

Polished sections of cut samples of phosphorite slabs and nodules (Figure 5) show massive, dense to porous and mottled internal structures (Figures 5a–5d), and concentric growth patterns around a nucleus in nodules (Figure 5e). The nodules are usually of centimeter size (up to 6 cm diameter), subspherical, and black to brown. The laminae are porous, from sub-mm to mm thick, with laminar to columnar textures. The nucleus of these nodules is composed of millimeter to centimeter angular fragments of pale-brown-pink phosphorite slabs (Figure 5e). The layers in the phosphorite nodules are composed of CFA with interlayered lamina containing abundant Fe-Mn oxyhydroxides that show high backscatter under the electron microscope (Figure 6j and anal. DRR38-2c supporting information Table S2).

The phosphorite slabs frequently form large pavement-like plates up to several decimeters long and up to 10 cm thick (Figure 5a). The phosphorites vary in color from white to a wide range of browns, and reddish and pinkish in some rocks. Slabs show dissolution and boring cavities infilled by carbonates and semiconsolidated sediment. The phosphorite slabs are usually encrusted on their top surface by millimeter-thick, rarely centimeter-thick, hydrogenetic Fe-Mn crusts, and hosting benthic organisms (cold-water corals, bryozoans) (Figure 5a). Fe-Mn replacement of the margins of the slabs is common and may extend to the interior of the phosphorite slabs, especially across fractures and along bored channels with development of dendritic features (Figures 5a and 5b). In some samples, brecciated textures are observed at the base of phosphorite with clasts (sand to pebble size) composed by phosphates cemented by and partially to completely replaced by Fe-Mn oxyhydroxides (Figure 5c).

Thin sections, polished sections, and electron microscope (EPMA) images of phosphorite slabs show large areas of microcrystalline apatite and CFA, also identified by XRD (Figure 6). In addition, calcite forms a micritic relict mosaic, being partially to completely replaced by phosphates. Isotropic collophane extensively replaced skeletal material and most of the calcite cement in the samples. Intergrowths of collophane with CFA are common. Calcite filling millimeter-sized to centimeter-sized cavities (borings) in the phosphorite slabs (Figure 5a) forms a microsparitic to sparitic mosaic. The percentage of bioclasts in the phosphorites range from zero to 65 vol %. Carbonate bioclasts are composed of phosphatized and well-preserved test fragments of planktonic and benthic foraminifera (Figure 6), including abundant globigerinoides, globigerinas, globigerinidos, and globorotalias with chambers filled by phosphate. The presence of sparse shell fragments of catalpsydra indicates an early Miocene age for some phosphorite slabs (e.g., sample DRR47-1). Occasionally, foraminifera chambers are filled by and the test replaced by Fe-Mn oxyhydroxides (Figure 6f). Nonphosphatic minerals are rare and mostly subangular to subrounded detrital quartz, feldspar, and clay

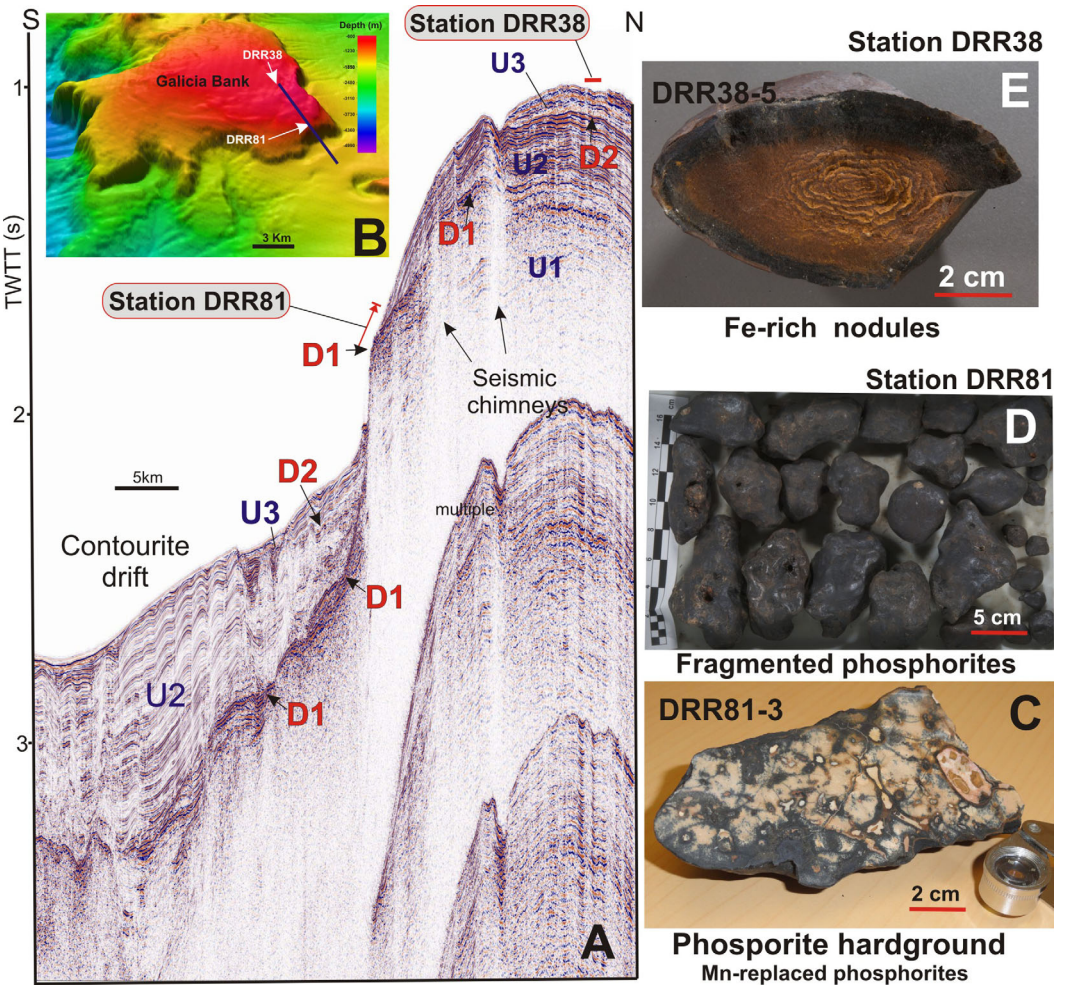

Figure 3. (a) S-N A10 multichannel seismic profile across the base and southern slope of Galicia Bank. Vertical exaggeration is X25 (V = 2.0 km/s). (b) Location of seismic profile and dredge stations. Phosphorites formed hardgrounds linked to the D1 discontinuity. (c) Phosphorite slab replaced in part by Fe-Mn oxides in veins along fractures; (d) A large suite of phosphorite pebbles; samples in Figures 3c and 3d were collected on the flanks of the bank. (e) Fe-rich nodule collected on the summit of the Galicia Bank in contourite deposits.

minerals. Different degrees of alteration are observed on the surfaces of some phosphorite slabs giving rise to the pseudomorphic replacement of phosphates by colloform Fe-Mn oxyhydroxides (Figure 6g).

The phosphorite slabs from station DRR81 on Galicia Bank and station DRR47 on Sancho seamount show comparable lithology, composition, and age of the limestone that was replaced. Depositional ages of CFA-replaced carbonates are predominantly middle Miocene and older (Table 3, see isotopic section below).

4.2.2. Fe-Mn Nodules and Crusts

Three types of Fe-Mn deposits have been recognized based on their structure, petrography, and mineralogy: Fe-Mn crusts, Co-rich Mn nodules, and Fe-rich nodules.

Polished cross sections of Co-rich Mn nodules show an internal structure of concentric laminae around a nucleus (Figure 5f). These nodules are usually centimeter size (up to 4 cm maximum diameter), subspherical to ellipsoidal, and black with submetallic luster. The nucleus is not visible under the microscope. The concentric laminae consist of an intimate intergrowth of poorly crystalline 10 Å manganates (todorokite, romanechite, and coronadite) and 7 Å manganates (birnessite) (supporting information Figures S3c and S3e). Asbolane may be an accessory mineral. Intercalated lamina of Mn carbonates identified with EPMA show low backscatter whereas the Mn-oxide lamina show high backscatter (Figure 7c and anal. DRR81-1-8 supporting information Table S3). Abundant well-preserved carbonate bioclasts (miliolidae, other foraminifera, and abundant radiolarians) are dispersed in the layers. The chambers of foraminifera are filled by fibrous Mn oxides (Figure 7d). Microfractures filled with micritic to sparitic calcite crosscut the Fe-Mn layers. The

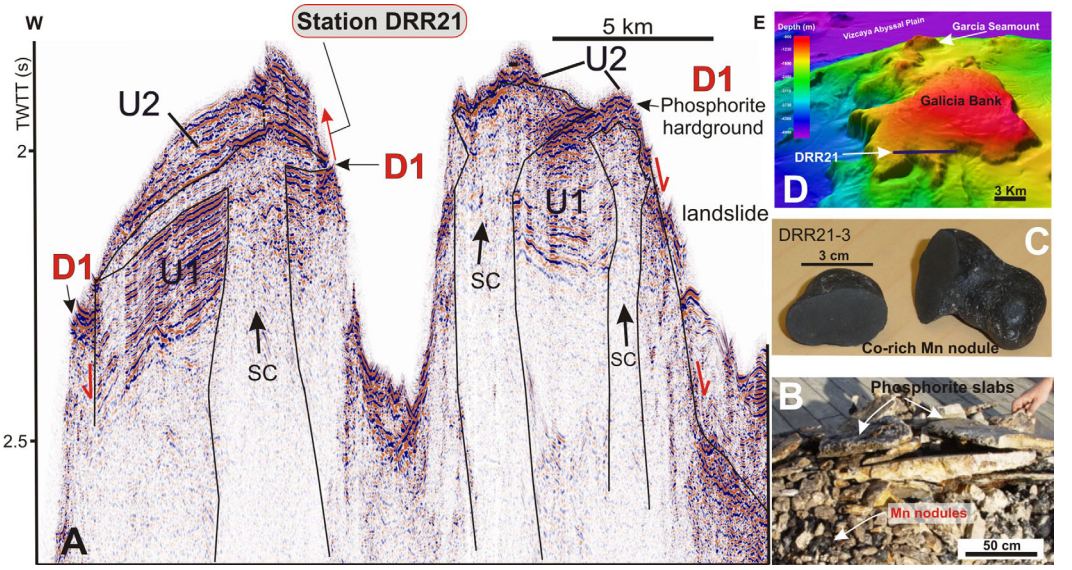

Figure 4. W-E A05 multichannel seismic profile across mounds and canyons along southern Galicia Bank. Vertical exaggeration is X18 (V = 2.0 km/s). Mounds with an internal chaotic and indistinct seismic reflection pattern and development of "seismic chimneys (SC)" that crosscut the D1 discontinuity and affect U1 and partially U2 units. (b) Suite of phosphorite slabs and Co-rich Mn nodules dredged at station DRR21. (c) Cut sections of Co-rich Mn nodules. (d) Location of seismic profile and dredge station.

percentage of bioclasts ranges from 1 to 20% with an average of 10 vol %. Dispersed detrital grains of quartz are visible under the microscope.

Fe-rich nodules are centimeter-size brown to orange concretions (5 cm maximum diameter) with variable shapes (subspherical to irregular; Figure 5g). These nodules show concentric laminae, but tabular samples with a complex arrangement of layers are also common. The nuclei cannot be differentiated from the layers under the microscope. These nodules are composed of goethite and lepidocrocite (Figure S3f) forming a microcrystalline ($<12\ \mu$m) mosaic of crystals with rhomboidal cross sections (Figures 7e and 7f). In addition, detrital grains of quartz, feldspar, and clay minerals are dispersed in the nodules. Framboidal pyrite, partially to completely replaced by Fe-oxyhydroxides, occur in some samples (Figure 7f). These framboids, with a diameter less than 25 μm and formed by several idiomorphic to subidiomorphic crystals, commonly fill chambers of foraminifera. The surface of some Fe-rich nodules is stained by thin black-brownish Fe-Mn crusts.

Black Fe-Mn oxyhydroxide crusts (Figures 5a–5d) show a continuous succession of subparallel laminae covering rock substrates (nodules, phosphate pavements, and basement or drop stones of igneous, metamorphic and sedimentary rocks). The Fe-Mn crusts vary in thickness from a patina to several centimeters. Thin Fe-Mn crusts (Figure 5d) show a finely laminated structure with colloform laminar to columnar textures. They have the appearance of typical hydrogenetic crusts, with botryoids and current-smoothed upper surface, which indicate formation at the seafloor. The crusts are composed of poorly crystalline vernadite with minor amounts of other Mn oxides such as asbolane, and goethite is an accessory minerals.

The underside margin of phosphorite slabs are commonly replaced by todorokite and goethite, which also commonly infill fractures, giving rise to a thick, Fe-Mn layer with an apparent massive structure (Figures 5a–5c). These Fe-Mn-oxides are in part replacement layers of phosphorite that formed subseafloor and can be considered stratabound deposits.

4.3. Chemical Composition

4.3.1. Phosphorite Nodules and Slabs

Composition of phosphorite slabs (samples DRR47-1A, DRR81-3, DRR81-4, and DRR81-5B) and nodules (sample DRR38-2) from different dredge sites are summarized in the Table 1. The P_2O_5 contents of the phosphorites range from 22 to 32.6 wt %. Phosphatization is more pervasive on Galicia Bank with P_2O_5 contents of more than 30 wt % at stations DRR-38 and DRR-81 and lowest on Sancho seamount (DRR-47 station). The CaO/P_2O_5 ratios range from 1.21 to 2.18. These values indicate intense phosphatization, especially those

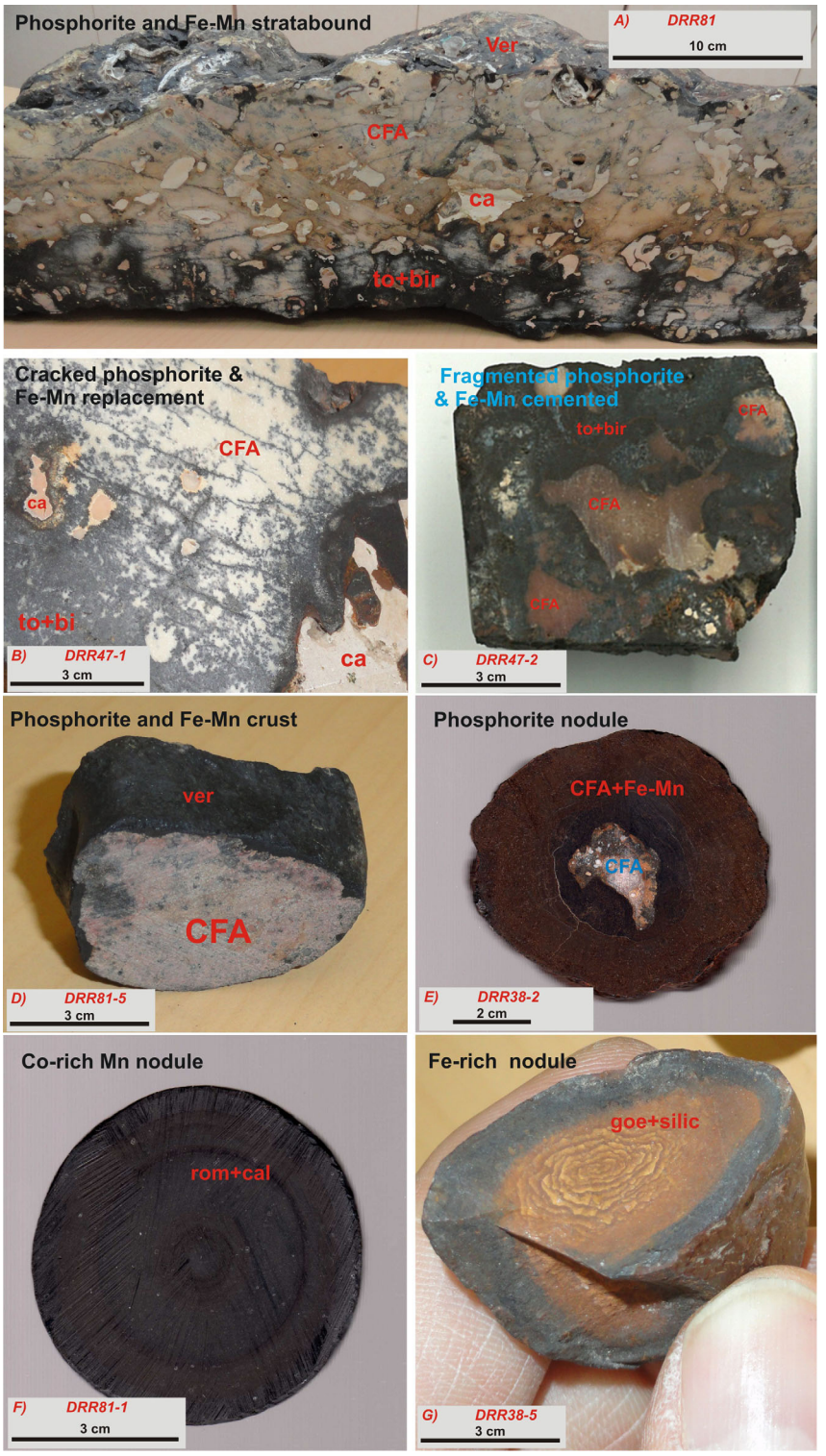

Figure 5. Suite of mineralization types from the Galicia Bank region. (a) Cross section of a phosphorite slab composed of dense CFA and showing replacement by Mn oxides (todorokite (to) and birnessite (bi)) along the underside margin and along fractures, and thin patina of hydrogenetic vernadite (ver) coats the upper surface; later-stage CFA and carbonate (Ca) fill cavities. (b and c) Cross section of phosphorite slabs showing parallel fracture set and partial replacement by Fe-Mn oxides in Figure 5B and pervasive replacement in Figure 5C; cavities are filled by CFA and carbonate. (d) Phosphorite fragment with an ~5 mm thick hydrogenetic Fe-Mn crust. (e) Cross section of spheroidal phosphorite nodule composed of a phosphorite nucleus and concentric layers of CFA and Fe-Mn oxides. (f) Cross section of concentric layers of Co-rich Mn nodule comprized of romanechite (rom) and calcite bioclasts (cal). (g) Fe-rich nodule formed by goethite (goe) and silicates (silic) showing well-developed concentric pattern.

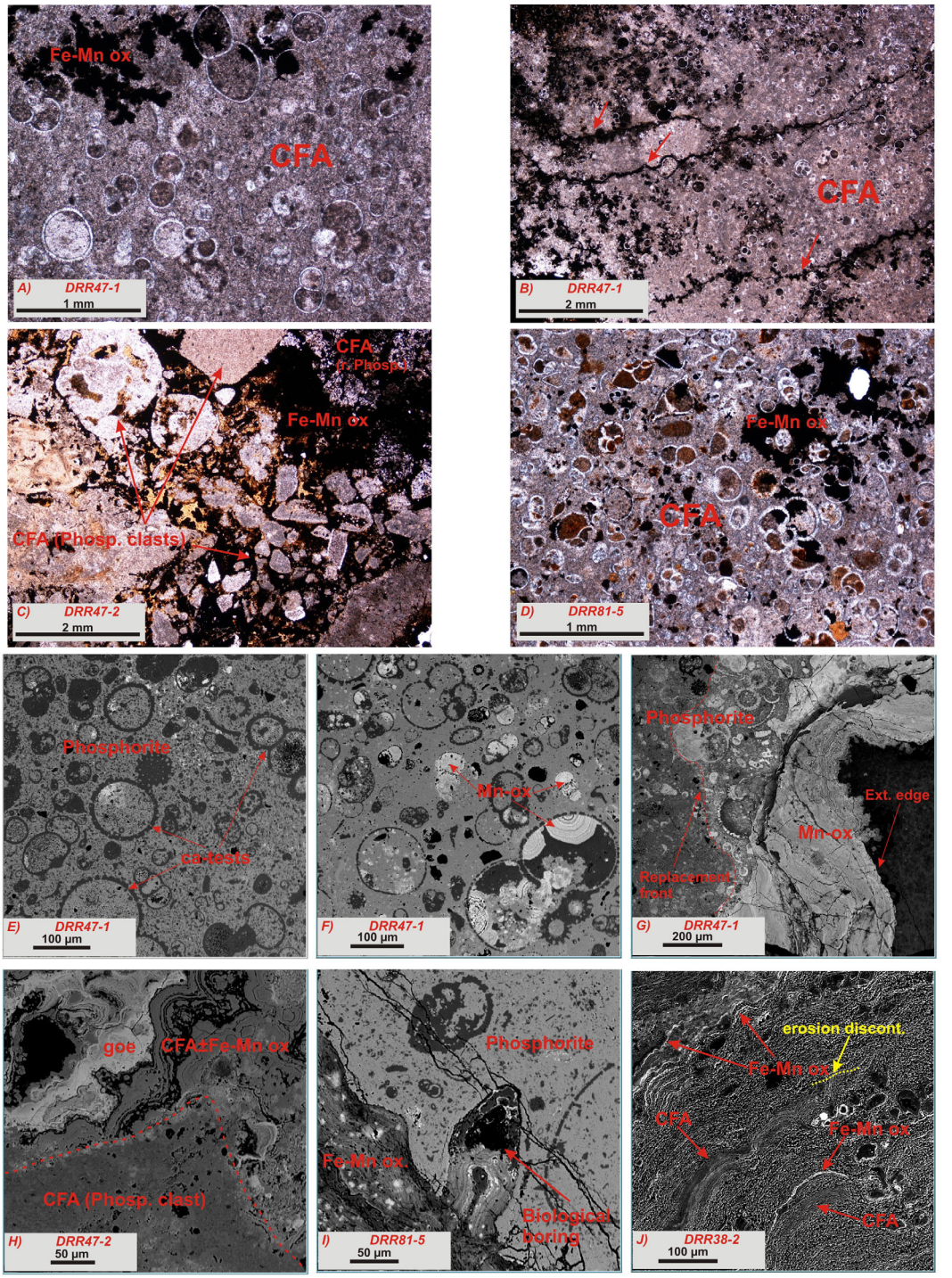

Figure 6. Thin and polished-section photomicrographs of phosphorite. (a and b) Sample from Sancho seamount with abundant foraminifera and fractures, some microfossil chambers, and patches filled by dendritic Fe-Mn oxides; (c) brecciated phosphorite from Sancho seamount with interclast cement composed of todorokite and birnesite (Fe-Mn ox) and matrix composed of Fe-Mn replaced phosphorite (r. Phosp.). (d) Phosphorite from Galicia Bank rich in Miocene foraminifera, with some patches and chamber fill of Fe-Mn oxides. (e–g) EPMA photomicrograph of foraminifera chamber fill by Fe-Mn oxides and CFA replacement fronts; ca-test = calcite tests; in Figure 6g, a sharp replacement front of Fe-Mn oxides replacing the phosphorite. The external Mn-oxide layer is lining a cavity. (h) EPMA photomicrograph of phosphorite breccia clast cemented by Fe-Mn oxyhydroxides and CFA cavity fill. (i) EPMA photomicrograph of phosphorite slab top-side edge with biological boring and patina of hydrogenetic Fe-Mn crust (Fe-Mn ox.). (j) EPMA photomicrograph showing the concentric pattern of CFA and Fe-Mn oxides in a phosphorite nodule from Galicia Bank.

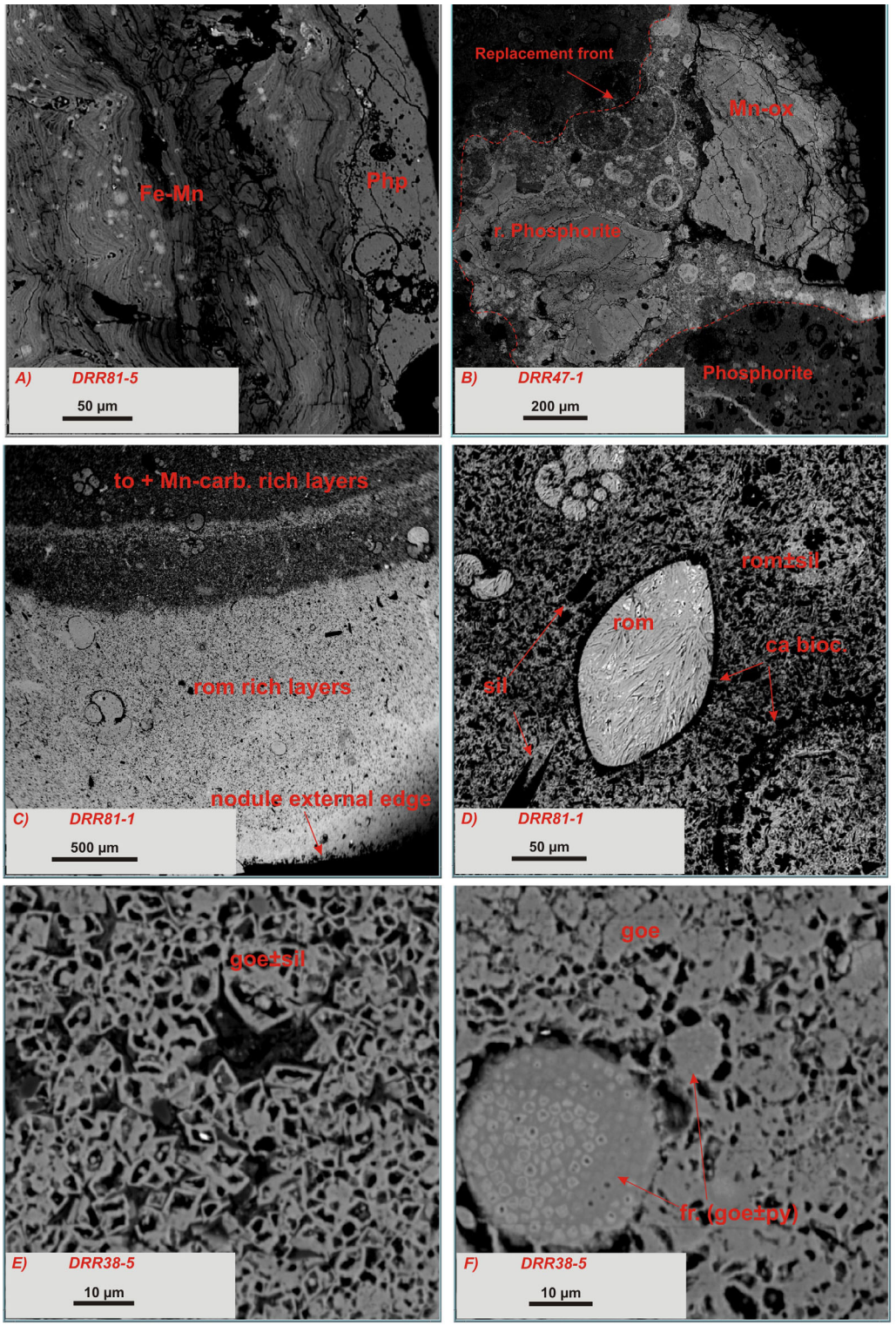

Figure 7. Thin and polished-section EPMA photomicrographs of Fe-Mn deposits. (a) Laminated hydrogenetic Fe-Mn patina composed of vernadite encrusting phosphorite (Php). (b) Fe-Mn replaced phosphorite (r. Phosphorite) showing the oxide mineralization front that cross-cuts a foraminifera test; Mn-ox is a thin cavity lining of Mn oxide. (c) Succession of romanechite-rich (rom) and todorokite-rich layers (to) in a Co-rich Mn nodule; note the relict microfossils. (d) Detail of romanechite-rich layer with dispersed silicates (sil) and carbonate bioclasts (ca bioc.) filled by fibrous romanechite. (e) Rhombohedral mosaic of goethite (goe) in an Fe-rich nodule; the skeletal rhombs may have been siderite replaced by goethite. (f) Framboidal texture in pyrite partially replaced by goethite (fr. (goe ± py)).

close to $CaO/P_2O_5 = 1.32$, characteristic of pure fluorapatite [*Manheim and Gulbrandsen*, 1979]. Fluorine contents exceed 2% in some samples reflecting the abundance of CFA and need for charge-balancing elements. The F/P_2O_5 ratio (0.06) is closer to the fluorapatite end member (0.089) than to the most substituted francolite (0.148) end-member of the range [*McClellan and Van Kauwenbergh*, 1990]. The SO_4^{2-} contents (0.12–1.64%) are lower to slightly greater than the maximum amount (1.2% SO_4^{2-}) thought to typically substitute for PO_4^{3-} in CFA. The SiO_2 contents are low (less than 4.8 wt %) and SiO_2/Al_2O_3 ratios range from 1.21 to 3.25, reflecting the presence of aluminosilicates. Total organic carbon (TOC) is less than 0.4 wt % indicating minor organic matter. Total REY vary widely, from 73 to 1938 μg/g (Table 1) with a mean of 1017 μg/g. The lowest total is for phosphorite slab DRR47-1A and the highest is for phosphorite nodule DRR38-2. The Ce/La ratios range from 0.23 to 0.76, except for sample DRR38-2, which is 3.35. These Ce/La ratios except the last one are similar to the ratios for seawater, indicating that the REY and phosphate host were derived from seawater, probably within or near an oxygen minimum zone. Finally, the Ce/La ratios 0.71 (sample DRR47-2) and 3.35 (sample DRR38-2) are higher than ratios found in seawater at any depth, and probably reflect the postdepositional influence of hydrothermal fluids. Shale-normalized REY patterns [*Piper*, 1974a, 1974b] support derivation of the REY and phosphorites from seawater (Figure 8). The characteristic patterns are HREY enriched, strong negative Ce anomaly and positive Gd and Y anomalies, which are found for all the samples except the phosphorite nodule DRR38-2, which shows a strong positive Ce anomaly (Figure 8).

The phosphorite nodule DRR38-2 has intercalations of Fe-Mn oxides with phosphatic laminations, which is reflected in the high Fe and Mn contents. All phosphorite samples with high Fe and Mn show higher trace metal (e.g., Co, Ni, Pb, and Ba) and REY contents, especially notable in sample DRR47-2: Ni (0.38 wt %), Ba (0.16 wt %), Co (0.14 wt %), Cu (0.09 wt %), and HREY (878 μg/g). These contents are similar to those for sample DRR47-1B in Table 2: Ni (0.86 wt %), Co (0.37 wt %), Ba (0.21 wt %), Cu (0.15 wt %), and HREY (368 μg/g). Both samples are interpreted to be stratabound Fe-Mn layers formed by different degrees of replacement and impregnation of phosphorite slabs. The degree of replacement increases progressively from the interior to the margin and along fractures in the phosphorites, progressively increasing the contents in Fe, Mn, Ba, Pb, Cu, and other metals and decreasing P and Ca (anal. DRR47-2-12, DRR47-2-3, and DRR47-2-4 in supporting information Table S2).

4.3.2. Fe-Mn Nodules and Crusts

Fe-Mn stratabound DRR47-1B layer and crust DRR81-5A show moderate MnO (23.3 and 27.6 wt %) and Fe_2O_3 (15.4 and 23.8 wt %) contents, with Mn/Fe ratios of 1.7 and 1.3 for the bulk samples (Table 2). The crust shows higher TiO_2 and much lower CaO and P_2O_5 than sample DRR47-1B. With respect to trace elements, Co (0.85 wt %), Pb (0.28 wt %), and Tl (81 μg/g) are relatively enriched in the crust sample, whereas Ni (0.86 wt %), Ba (0.2 wt %), and Cu (0.15 wt %) are higher in the stratabound layer; contents of the other elements are similar for both samples. From an economic standpoint, Ni and Co are significantly high in the stratabound layer and crust, respectively. The sum of concentrations of potential ore metals (Cu, Co, Ni, V, and Mo) are 1.5 and 1.7 wt % for bulk samples, respectively. The total REY contents are 894 μg/g for sample DRR47-1B and 1644 μg/g for crust DRR81-5A. The most striking features of the REY patterns for these samples are the negative Ce anomaly for the stratabound sample and strongly positive Ce anomaly for the crust (Figure 8). In addition, both samples show positive Gd anomalies. The Y/Ho ratios vary over a wide range (13–36), typical of hydrogenetic crusts and hydrothermal manganese deposits in the Pacific Ocean [*Hein et al*., 1997], indicating that Y and Ho are fractionated in the marine environment [*Bau et al*., 2014].

Bulk Co-rich Mn nodules have high MnO contents (up to 58 wt %) and low Fe_2O_3 (down to 0.42 wt %). The Mn/Fe ratios vary from 45 to 153. The contents of other major elements are low except for CaO (up to 16.2 wt %), Ba (to 5.9 wt %), and MgO (to 2.90 wt %). The markedly high Ba contents reflect the abundance of romanechite rather than the presence of barite, which was not detected by EPMA, optical microscopy, or XRD analyses (supporting information Figures S3c and S3e). The abundance of Pb in some nodules may be due to sorption on the Mn oxides or formation of a minor amount of coronadite or other Pb-rich Mn oxide (Figure S3e). The total concentrations of potential ore metals (Cu, Co, Ni, V, Mo, W) are 2.4, 2.3, and 1.3 wt % for bulk nodules DRR81-1, DRR21-1, and DRR21-2, respectively. From an economic standpoint, Co contents in two of the nodule samples are remarkable high, among the highest measured in nodules [*Hein et al*., 2013; *Hein and Koschinsky*, 2014]. The distribution patterns of REY show small variations in total contents (Table 2) with LREE being most abundant in all the samples. The REY plots of Co-rich Mn nodules show strong positive Eu and Ce anomalies and little fractionation between LREY and HREY (Figure 8).

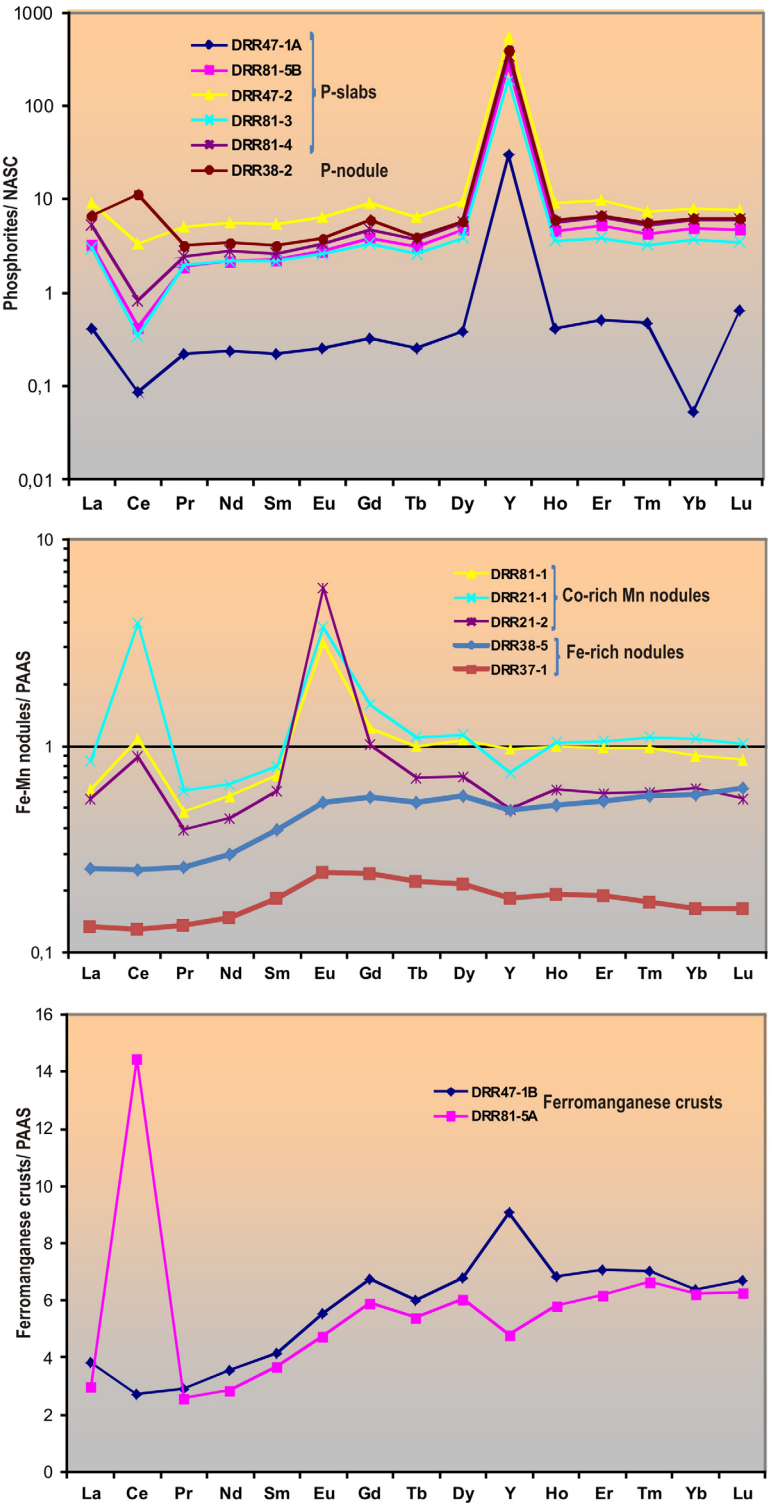

Figure 8. PAAS-normalized and NASC-normalized REY element plots for phosphorites, Co-rich Mn nodules, Fe-rich nodules, and Fe-Mn crusts.

Iron is the most abundant element in the bulk Fe-rich nodules followed by Mn, Si, Mg, and Al (Table 2), with Mn/Fe ratios of 0.03 and 0.09. Boron, As, Co, Ni, Sr, and Ba are the most abundant trace elements. The average concentrations of other trace elements (Cr, Cu, Li, Nb, Pb, Rb, Sc, Se, and W) are not higher than 30 μg/g with Ag, Sb, and Tl below detection limits. The total concentrations of potential ore metals (Cu, Co, Ni, V,

and Mo) are very low as are the REY contents (ΣREY < 67 μg/g). REY patterns show positive Eu anomalies and no Ce anomaly. The patterns also show a moderate HREY enrichment and there is LREY/HREY fractionation especially in nodule DRR38-5 (Figure 8).

4.4. Isotopes

The samples have Sr and Nd isotope values ranging from 0.708160 to 0.714808 for $^{87}Sr/^{86}Sr$ and -8.58 to -10.71 for ε_{Nd} (Table 3). Significant differences in the Sr isotope ratios exist between the CFA-dominant phase in phosphorites (from 0.712385 to 0.714808) and their pristine relict calcite precursor (0.708160–0.708611). Apparent maximum ages of phosphatization were determined using the Sr isotope composition of the carbonate that was not phosphatized, the seawater Sr isotope curve of *McArthur and Howarth* [2004], and assuming that phosphatization took place soon after carbonate sedimentation. This assumption is in accord with what is known about the formation of typical phosphorite hardgrounds in modern continental-margin settings [e.g., *Burnett*, 1977; *Bentor*, 1980; *Birch*, 1980; *Froelich et al*., 1988; *Glenn and Arthur*, 1988; *Burnett and Riggs*, 1990; *Follmi*, 1990]. Sr isotopes for pristine calcite in three phosphorites indicate depositional ages from 24.85 ± 0.9 to 17.7 ± 0.9 Ma (late Oligocene to early Miocene); the CFA shows the most radiogenic values (average 0.713551). These radiogenic Sr ratios may reflect deep-seated fluids venting in the area of Galicia Bank; the heat source for these hydrothermal fluids would have been geothermal rather than magmatic. Leaching of granodioritic-granitic basement rocks (Ossa Morena rocks) can explain the high Sr isotope values. The possibility that the aluminosilicate fraction is the cause of the Sr isotopic ratios and isotopic-derived apparent ages is not viable because of their low content in the samples; the Fe-Mn oxides in the phosphorites could have Sr isotope ratios that would lower the apparent Sr isotopic age. Phosphorite sample DRR47-2, strongly Fe-Mn oxide replaced, could have a questionable isotope-derived age, whereas the other phosphorites were selected to avoid this contaminant, verified by the low Fe and Mn contents (Table 1).

Nd and Sr isotopes are powerful tools for exploring paleoenviromental changes [*Palmer and Elderfield*, 1985a,b; *Stille et al*., 1996], and the Nd isotopic signature of Fe-Mn oxides indicates the sources of these oxides. For samples analyzed here, these isotopes do not show a marked similarity to those of the modern seawater masses in the area, corroborating that these are not recent deposits. The ε_{Nd} values measured for the leached Fe-Mn oxide fractions vary from -8.86 for Fe-rich nodules to -9.15 for Co-rich Mn nodules, higher the current range of NE Atlantic seawater in this region. The ε_{Nd} signatures of CFA vary from -9.54 to -10.71, above the values than present-day NE Atlantic seawater.

5. Discussion

Data presented here allow us to determine the Cenozoic succession of mineralization preserved on Galicia Bank: (1) phosphorite slabs and nodules, (2) Fe-Mn crusts and stratabound layers, (3) Co-rich Mn nodules, and finally (4) Fe-rich nodules. In addition, for each type of mineralization, we constraint the ages of formation and determine the influence of global and regional environmental/oceanographic conditions on the mineralization. We find that major changes in the oceanographic regime in the North Atlantic Ocean during the Cenozoic, driven by intraplate tectonism leading to the establishment of deep water exchange between the Artic and North Atlantic Oceans, played a role in the mineralization. The integration of mineralization, tectonics, and oceanography/paleoceanography allow for a comprehensive understanding of this continental-margin type of mineralization, which has generally not been well studied from the modern ocean basins.

5.1. Late Oligocene-Early Miocene Phosphorite Slabs

Like other global ocean locations [e.g., *Bentor*, 1980; *Baturin*, 1982; *Hein et al*., 1993; *Jones et al*., 2002; *Arning et al*., 2009], the phosphorites from the Galicia Bank region show a wide variety of morphologies, for example, nodules and pavements, and formation by the replacement of carbonate rocks and sediments by CFA.

5.1.1. Age Constraints of Phosphatization and Global Significance

Depositional ages of the carbonate component of the phosphorites from Galicia Bank (station DRR81) and Sancho seamount (station DRR47) (Table 3) were determined using Sr isotopes and micropaleontology. Three intervals (Figure 9) showed ages of late Oligocene ($\sim$25.7–24 Ma), early Miocene (23.8–22.6 Ma) for Galicia Bank and early Miocene (18.6–16.8 Ma) for Sancho seamount; it is likely that carbonate sedimentation was continuous during that entire time interval. The timing of phosphatization is not known because

the Sr isotopes of the CFA have been modified by the mineralizing fluids. The REY pattern of the phosphorites (Figure 8) reflect that of seawater [*DeBaar et al*., 1985], indicating precipitation from cold seawater. If phosphatization was early diagenetic, then the carbonate depositional ages (late Oligocene-early Miocene) may closely approximate the phosphatization ages. This assumption is supported by phosphatization of seabed surface sediment that formed hardground—this type of early-stage phosphatization is characteristic of continental-margin phosphorite deposits [e.g., *Glenn and Arthur*, 1988]. If true, then phosphatization was comparable in age with the major Cenozoic phosphatization events determined for other phosphorite deposits in the global ocean [*Hein et al*., 1993]. These events of phosphatization corresponded to times of climate transitions from glacial to warm in the late Oligocene-early Miocene [*Hein et al*., 1993].

Phosphorites on Galicia Bank were likely produced by processes that characterize phosphorites forming today along continental margins. Marine phosphorites along continental margins typically form by replacement of and cementation of carbonate sediments at or near the seafloor [e.g., *Burnett*, 1977; *Burnett and Riggs*, 1990; *Bentor*, 1980]. These phosphorites commonly form hardgrounds, nodules, pebbles, and slabs, such as is found forming today off the Peru-Chile margin [e.g., *Froelich et al*., 1988; *Glenn*, 1988]. The phosphate is supplied to the sediment by organic matter produced during moderate to high primary productivity as a result of upwelling. Winnowing by bottom currents of the phosphate sediment can produce more pure phosphorites free of siliciclastic and biogenic materials. Winnowing can produce pure phosphorite lag deposits that may then transform into phosphorite hardgrounds through CFA cementation [e.g., *Föllmi*, 1996; *Filippelli*, 2011]. In addition, deep-sea waters may have acted as a reservoir for dissolved P and other nutrients during stages of climatic stability and sluggish oceanic circulation. During glacial periods, the P from the deep-sea reservoir may have been redistributed by upwelling into shallower waters around seamounts and banks due to enhanced global oceanic circulation as a consequence of the increased pole-to-equator thermal gradient. This process may have augmented the nutrients supplied to the upwelling system and further increased primary productivity in surface waters, increased the supply of biophosphate, and enhanced the expansion of the OMZ around topographic highs [*Hein et al*., 1993; *Koschinsky et al*., 1997].

These examples indicate that phosphogenesis occurred in the equatorial Atlantic and equatorial Pacific Oceans during the same time intervals [*Hein et al*., 1993; *Jones et al*., 2002]. Therefore, it can be inferred that strong upwelling occurred also in the northeast Atlantic during these late Oligocene to early Miocene phosphogenetic events. Although we have not sampled phosphorite of late Eocene to early Oligocene age in the Galicia Bank area, as occurs in the Pacific Ocean [*Hein et al*., 1993], we do not disregard the possible occurrence of phosphatization during that period because chalk samples with middle Eocene coccoliths were reported by *Black* [1964] near Station DRR81.

5.1.2. Paleoenvironmental Conditions and Constraints

The types of foraminifera and radiolarians reflect the paleoceanographic conditions that prevailed around Galicia Bank during phosphatization. Foraminiferal assemblages within phosphorites, such as the occurrence of *Austrotrillin*, indicate deposition of limestone in shallow water during the early Miocene (~24–23 Ma), before the bank began to subside. The occurrences of radiolarians and globular planktonic foraminifera (e.g., *Globigerinoides)* indicate that the bank was connected to the open ocean. Moreover, abundant radiolarians indicate high productivity waters around the bank due to upwelling.

The replacement of carbonate minerals by CFA is favored by the high concentrations of P in the pore waters of carbonate sediment and suboxic redox conditions. For example, sulphur bacteria, which contain large amounts of intracellular polyphosphates, can drive precipitation of CFA in suboxic-anoxic sediments [*Schulz and Schulz*, 2005]. They derive energy by oxidation of sulphide using nitrate or oxygen as the electron acceptor. Apatite replacement of carbonate by microbially mediated enzymatic reactions promotes PO_4^{3-} release from organic matter and CO_3^{2-} and Ca^{2+} release from carbonates by dissolution via organic acids [*Lamboy*, 1993]. The fact that Galicia Bank was located relatively close to the Iberian margin indicates that plankton-derived organic matter supplied the phosphate to the sediments. In addition, Galicia Bank and neighboring seamounts should have supported obstructional upwelling as water masses impinged on those edifices, which would also have promoted upwelling and associated productivity in surface waters. Strong upwelling is supported by the abundance of foraminifera and radiolarian found in the phosphorites (Figure 6 and Table 3). Barium, Cu, and Zn are enriched in the phosphorites from high productivity regions (e.g., Peru and Namibia margins) with an important contribution of plankton-derived organic matter [*Price*

and Calvert, 1978; *Froelich et al*., 1988]. However, moderate concentrations of these elements in the phosphorites of Galicia Bank (Table 1) are related to Fe-Mn replacements and encrustations rather than the involvement of marine plankton.

The low ε_{Nd} values of phosphorites may be explained by exchange between nonradiogenic bottom waters and surface waters caused by upwelling of cold, nutrient enriched water. Most $\varepsilon_{Nd(0)}$ values of phosphorites (Table 3) fall in the range of −7 to −9, characteristic of North Atlantic waters extant from 25 to 17 Ma [*Stille et al*., 1996]. However, the progressive decrease in $\varepsilon_{Nd(0)}$ from −8 to −9 for the first phosphatization event during the late Oligocene-early Miocene (25–22 Ma) to −10.71 in the late-early Miocene event (18–17 Ma) can be explained by the progressive increasing influence of the Northern Component Water (NCW) promoted by the formation of the northern gateways, the Greenland-Scotland-Ridge [e.g., *Müller-Michaelis et al*., 2013]. This is discussed further in the next section.

5.1.3. Proposed Genetic Model

Most published phosphogenetic models address phosphorites that formed in organic-matter-rich environments, particularly areas of strong upwelling along highly productive continental margins (e.g., Peru and Namibian margins). On the other hand, there are few reports dealing with phosphorites that formed in moderate to low-productivity environments with organically poor host sediments [*Hein et al*., 1993; *Benninger and Hein*, 2000]. We suggest that formation of phosphorites on Galicia Bank fit a genetic model that includes parts of both of these models. It is well known that phosphatization is favored under suboxic conditions because P is enriched in suboxic-anoxic sediments by early microbial degradation of organic matter, and several redox reactions that occur at various depths in the sediment: sulphate-reduction, sulphide-oxidation, and Mn and Fe oxide dissolution and release of incorporated P [e.g., *Burnett and Riggs*, 1990; *Schulz and Schulz*, 2005; *Filippelli*, 2011]. Fe-Mn-oxide formation is favored under more oxic conditions. If bottom waters become anoxic, phosphorite typically forms at the upper and lower margins of the anoxic OMZ, such as off the Peru-Chile margin [e.g., *Glenn and Arthur*, 1988]. The redox cycling of Fe-Mn oxyhydroxides may play an important role in concentrating phosphorous around Galicia Bank as reported for other areas with discontinuous and moderate upwelling [*Jarvis*, 1992; *Benninger and Hein*, 2000]. Our phosphogenesis model follows this sequence: (1) carbonate sediment accumulated on Galicia Bank during the Oligocene and early Miocene, possibly also the Eocene. Dissolved phosphate in seawater concentrated in a suboxic OMZ when Galicia Bank was still in relatively shallow water, too shallow for the formation of hydrogenetic Fe-Mn deposits. The sources of dissolved and colloidal Fe were from the Iberian continental margin and from leaching of basement rocks by geothermally driven circulation of fluids. This colloidal Fe provided a substrate for the sorption of P, adding to the available P pool; (2) this suboxic, P-rich environment was ideal for the early diagenetic replacement of the carbonate sediment, which was phosphatized from pore fluids below as well as at the seafloor where the OMZ intersected the bank. This phosphatization produced mineralization fronts that crosscut depositional fabric (Figures 5a and 6g). The result of phosphatization was the formation of a hardground, which constitutes the phosphorite slabs described here; (3) after additional subsidence of the bank, and boring of the hardground by benthic fauna, Fe-Mn deposits formed and through diagenetic processes replaced the margins of the phosphorite slabs and areas adjacent to fractures and other porosity; (4) at this stage, redox recycling of Fe-Mn oxides and bacterially mediated reactions (e.g., sulphide oxidation by *Thiomargarita*) [*Schulz and Schulz*, 2005] likely precipitated additional phosphorite; parts of the older phosphorite and Fe-Mn deposits were redistributed and in the process concentrated economically important metals. These recycling and diagenetic processes are important in the formation of phosphorite in organic-matter-poor environments [*O'Brien and Heggie*, 1988; *O'Brien et al*., 1990].

The presence of radiogenic Sr in phosphorites (ratios up to 0.7148) indicates participation of mineralizing fluids that imprinted their isotopic Sr signature in the phosphorites. We interpret these changes to be related to input of hydrothermal fluids that may have also promoted remobilization and precipitation of phosphates as observed in brecciated samples (Figure 6h). These hydrothermal inputs are addressed in section 5.3.3.

The phosphate nodules show internal discontinuities (Figure 6j) linked to erosion by currents probably associated with sea level low stands during global cooling, which was common in the middle Miocene [*Vincent and Berger*, 1985; *Flower and Kennet*, 1993]. The presence in the nodule of botryoidal fluorapatite and CFA, atypical of marine phosphorites, may indicate primary precipitation of phosphates in the sediments or phosphate replacement of Fe-Mn oxyhydroxides. In this way, the high contents in Fe, Mn, and trace metals

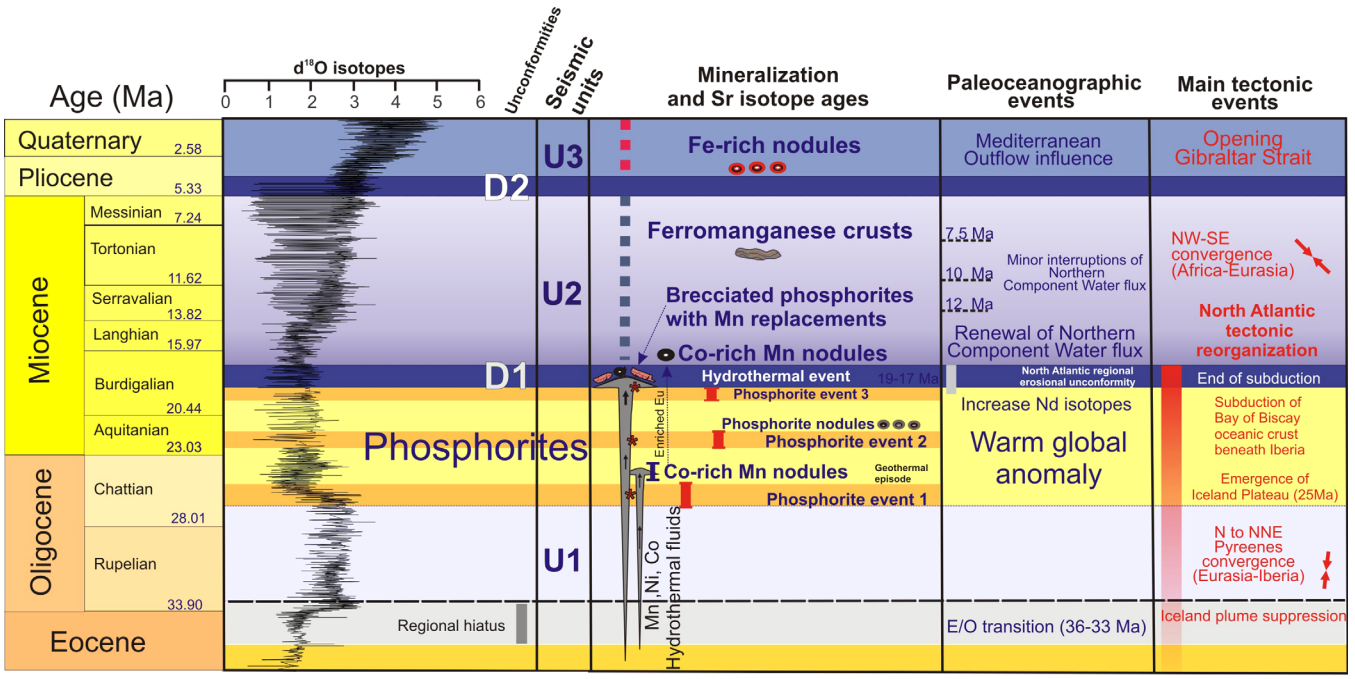

Figure 9. Schematic model for different types of mineralization in the Galicia Bank region and age sequences of tectonic and oceanographic events. The asterisks represent the Sr inferred ages for mineralizations. See text for detailed explanation.

can be explained either by phosphate replacement of Fe-Mn oxyhydroxides or by the diagenetic intergrowth of Fe-Mn oxide layers in the nodule. The nucleus of this nodule is an older phosphorite fragment. Fragmented phosphorite can be interpreted to result from brecciation of older phosphorites through gravity mass movement or tectonic processes during the Miocene, generating the nuclei for growth of new phosphorite and Fe-Mn nodules (Figure 9).

5.2. The D1 Unconformity: A Significant Early Miocene Paleoceanographic and Tectonic Reorganization in the North Atlantic

Based on the seismic profiles combined with the location of the dredge stations (e.g., Figure 3), we correlate the high reflective D1 unconformity with the phosphatized hardground. The age of this hardground is constrained by the age of the host sediment dated by Sr isotopes as latest early Miocene (17–16 Ma, Table 3 and Figure 9), and evidence for an early diagenetic origin for the phosphatization. This age correlates with a regionally significant unconformity preserved in North Atlantic deep water basins and dated from Faroe-Shetland Rockall Trough to Porcupine Bank as 19–16 Ma [e.g., *Stoker et al*., 2002; *Müller-Michaelis et al*., 2013]. This unconformity was first recognized in DSDP cores on Goban Spur and Rockall Trough [*de Graciansky et al*., 1984] and was related to vigorous bottom currents resulting from the introduction of Norwegian Sea Water along the North Atlantic margins. The Faroe Conduit developed in the early Miocene and was suggested to be the first true deep water connection between the Nordic Seas and the Atlantic [*Stoker et al*., 2005].

Therefore, we propose that the latest early Miocene D1 unconformity marks the abrupt end to the dominant phases of phosphogenesis, terminated by the marked changes in the oceanographic regime. The occurrence of a massive contourite drift mega-sequence (Unit U2, supporting information Figure S2) overlying this D1 unconformity confirms the establishment of vigorous bottom currents following the period of phosphogenesis. We suggest that these strong bottom currents were the result of the onset of the Northern Component Water (NCW) that impinged directly on Galicia Bank (Figure 10). Therefore, the submergence of the Greenland-Scotland Ridge resulted in locally vigorous deep water erosion as northern-sourced deep water flowed through the Faroe-Shetland Channel into the NE Atlantic [e.g., *Stoker et al*., 2002] (Figure 10).

The fact that the D1 unconformity is extensively faulted on Galicia Bank and Sancho seamount (supporting information Figure S1) suggests that tectonic reactivation occurred after termination of the main

phosphatization events and before deposition of the contourite drifts of Unit U2. This tectonic reactivation is linked to intraplate tectonism dated as early Miocene that occurred in the NE Atlantic, including the opening of the Faröe-Shetland Channel and Rockall Trough associated with significant basin subsidence [*Stoker et al*., 2001].

This tectonic event is reflected in the southern NE Atlantic margins as continent-ocean collision resulting in northward subduction of the Bay of Biscay oceanic crust beneath the Iberian continental crust. The age of this event, based on the age of the last deposits involved in the accretionary prism developed along the North Iberian Margin, was estimated to have been active until the Burdigalian (20.43–15.97 Ma) [*Alvarez-Marrón et al*., 1997]. Given these constraints, we suggest that the tectonic event affected Galicia Bank between the last main phosphatization event in the latest early Miocene (∼18–17 Ma) and the end of the subduction of the Biscay Bay at early/middle Miocene (∼15.97 Ma; Figure 9).

5.3. Early/Middle Miocene Geothermal Fluid Circulation, Co-Rich Mn Nodules, and Subseafloor Mineralization

We interpret the exceptional Co-rich Mn nodules and stratabound Mn replacement and encrustation of phosphorite deposits collected along the flanks and summits of seamounts from the Galicia Bank region as having formed through diagenetic processes. The circulation of mineralizing fluids was driven by geothermal heat, which produced metal-rich hydrothermal fluids. This suggestion is based on the uncommonly high Co contents in the nodules compared to hydrogenetic Fe-Mn nodules and crusts, the positive Eu anomaly, the Nd isotopic signature, and the Sr isotopes.

5.3.1. Age Constraints and Source of Mineralization

Mn-oxide mineralization occurred during at least two time intervals (Table 3 and Figure 10): early Miocene (23.8–22.6 Ma) for Galicia Bank Co-rich nodules and latest early Miocene (18.5–17.7 Ma) for Mn-oxide replacement of phosphorite slabs on Sancho seamount. These dates assume that Sr was derived mainly from seawater. The Co-rich Mn nodules were collected where the D1 phosphatized hardground was breached by chimneys, which represent fluid and sediment (diapir) upflow zones (Figure 4). The spherical shape of some of the nodules indicates that they formed either at the seafloor or within water-saturated unconsolidated sediment.

The seismic-defined chimneys crosscut sedimentary Unit U1, the D1 unconformity, and partially Unit U2. Even though it is difficult to discern on the seismic profiles, the seismic chimneys appear to be rooted in semitransparent acoustic facies interpreted to be black shale [*Vázquez et al*., 2008; *Vázquez et al*., 2009b]. A black shale at the base of the postrift Units (Albian-Cenomanian in age) has been described from Galicia Bank and surrounding regions [*Boillot and Malod*, 1988]. The shale is composed of homogeneous to laminated claystone and interbedded mudstone. Rising diapirs and associated fluid venting as a response to compressional tectonics could be driven by the viscosity of the black shale and abundant hydrocarbons. Black shales are known to be enriched in metals [e.g., *Vine and Tourtelot*, 1970], and this source can explain the high concentration of metals found in the Co-rich Mn nodules and stratabound Mn deposits. In addition, igneous rocks (granites and granodiorites) and possibly massive sulphides from the Ossa Morena basement of Galicia Bank may have been a supplementary source of metals for the mineralization at the seafloor. The Galicia Bank area nodules have higher Co than nodules from any other area of the modern ocean basin [*Hein et al*., 2015]. These remarkably high Co contents must have a source in addition to seawater and our proposal of leaching of black shale and/or basement rocks is a viable explanation.

Therefore, we propose that the abundant metals in the Co-rich Mn nodules and Fe-Mn stratabound deposits are related to fluid/sediment upflow structures driven by regional tectonic reactivation during the early and middle Miocene. In addition, geothermally driven fluid circulation along these structures promoted transport of metals for mineralization at and near the seafloor (Figure 10 and supporting information Figure S1).

5.3.2. Paleoenvironment

The Co-rich Mn nodules from the Galicia Bank region show predominantly spheroidal and cylindrical morphologies with abundant microfossils, indicating their formation near but below the water-sediment interface. Cylindrical nodules are similar to tubular concretions formed around burrows that occur in the Black Sea and the Gulf of Cadiz [*Baturin et al*., 2002; *González et al*., 2012]. It is likely that the cylindrical nodules grew around burrow tubes within sediments. The different types of nucleus in part determine the final

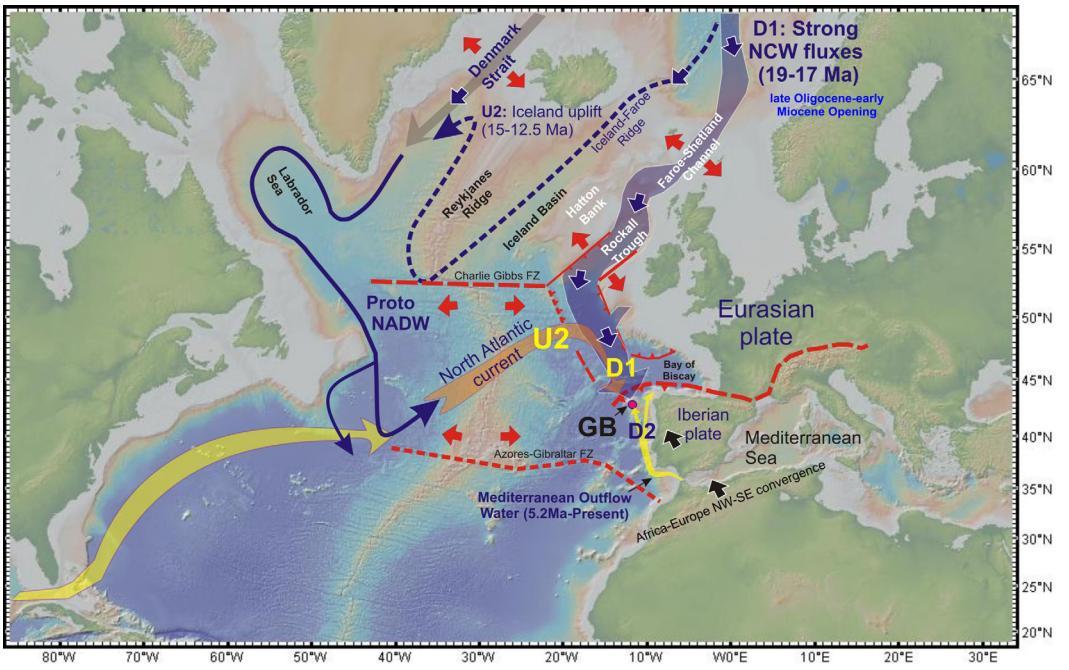

Figure 10. Paleoceanographic and tectonic events reconstruction of the North Atlantic at the time of mineralization of the Galicia Bank (GB) region.

morphology of the nodules, including nucleation associated with redox horizons. Foraminifer tests and detrital grains acted as nucleation sites for the spheroidal Co-rich Mn nodules in areas dominated by bioclastic sediments.

5.3.3. Proposed genetic Model

Typically, the precipitation of Mn oxides from hydrothermal fluids occurs below the water-sediment interface as stratabound layers and cement with a large fractionation between Fe and Mn [*Hein et al*., 1997; *Koschinsky and Hein*, 2003; *Hein et al*., 2005]. These processes occur when the oxides precipitate rapidly from low-temperature hydrothermal fluids (<120°C), which does not allow time for trace metals to be adsorbed by the precipitates. However, the oxide minerals can be enriched in one or more of Li, Mo, Zn, Pb, Cu, or Cr, rarely Co, based on the types of basement rocks leached, the composition of the fluids, and formation of mineral deposits deeper in the hydrothermal system [*Hein et al*., 1997]. The Co-rich Mn nodules from Galicia Bank are characterized by a submetallic luster, presence of 10 and 7 Å manganates, high Mn/Fe ratios, low REY contents, positive Eu anomalies, and moderate to high Mo, Pb, V, and Tl contents, all characteristic of hydrothermal Mn deposits from the modern ocean basins. The Mn nodules plot at the almost pure Mn-rich end-member (Mn/Fe 45–153) on the Mn-Fe-(Co + Ni + Cu) × 10 ternary diagram [*Bonatti et al*., 1972; *Lyle*, 1981; *Dymond et al*., 1984]. On the other hand, the very high Co (up to 1.8 wt %), moderate Te, and a positive Ce anomaly are unusual for hydrothermal Fe-Mn deposits. The positive Ce anomalies can be explained by the input of a hydrogenetic Fe-Mn component. This component can be identified using the REY plots of *Bau et al*. [2014], where the Co-rich nodules plot either in the hydrogenetic (seawater-sourced) field or between the hydrogenetic and hydrothermal fields (Figure 11). This dual source can also be seen in REY patterns that share features with both hydrogenetic deposits (positive Ce anomaly and negative Y anomaly) and hydrothermal deposits (positive Eu anomalies). Our data show that hydrothermal and hydrogenetic deposits form a continuum and that it does not seem to matter whether the hydrothermal system is geothermally or magmatically driven. Continuous REY scavenging from seawater would increase the REY concentrations and reduce the Y_{SN}/Ho_{SN} ratios with time; the Ce_{SN}/Ce_{SN^*} ratios would increase as long as the Co-rich Mn nodules were exposed to seawater.

The Sr isotopes of CFA in the phosphorite slabs (0.7123–0.7148) are anomalously high compared to Miocene seawater, which we interpret to reflect the hydrothermal-fluid component to the mineralized slabs (Table 3). The Sr isotopic values are characteristic of continental rocks and indicate that the leached source

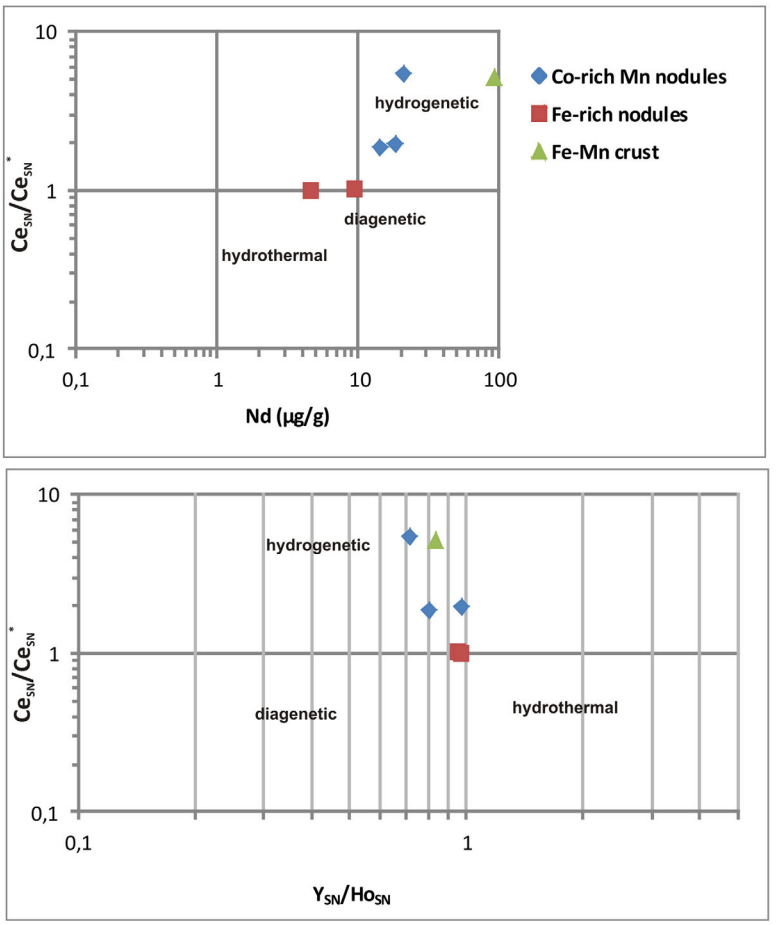

Figure 11. Plot of Fe-Mn deposits on graphs of Ce_{SN}/Ce_{SN} versus Nd concentration and Ce_{SN}/Ce_{SN} ratios (after *Bau et al*. [2014]). The samples plot into distinctive areas on these diagrams discriminating among the different genetic types of Fe-Mn mineralization. For further explanation see text.

rocks included either Mesozoic and Cenozoic terrigenous units of the Atlantic passive margin or Paleozoic granitic-granodioritic rocks of the Ossa Morena Variscan Zone that conform to the basement of Galicia Bank [*Capdevila and Mougenot*, 1988]. The Nd isotopes of the Fe-Mn mineralization show nonradiogenic values of 0.512169 ($\varepsilon_{Nd} = -9.15$) and 0.512198 ($\varepsilon_{Nd} = -8.58$). We interpret those values to represent either a hydrothermal mineralizing fluid sourced from a mix of continental crustal rocks, and/or a hydrogenetic component precipitated from North Atlantic seawater [*Stille et al*., 1996].

We suggest that besides the hydrothermal and hydrogenetic components in the Co-rich nodules, early-diagenetic remobilization of components disseminated in the sediment was facilitated by the hydrothermal fluids. The high contents of Mo and Ba are partly explained by this diagenetic remobilization. All these factors indicate a mixed hydrothermal-hydrogenetic-diagenetic origin for the Mn nodules.

The Fe-Mn stratabound layers and impregnations also reflect tectonic and hydrothermal processes. Their textures and mineralogy are indicative of a hydrothermal origin, brecciation by hydrofracturing, and Mn-oxide precipitation and replacement of the phosphorites (Figures 5b, 5c, 6b, and 6C; anal. DRR47-2, DRR47-2-12, DRR47-2-3, and DRR47-2-4 in supporting information Table S2). The intense brecciation of phosphorite may be related to formation of the chimneys (diapirs and domes) impacting the D1 phosphatized hardground shown on seismic profiles (Figures 3 and 4). Thus, we interpret these structures as having been produced by ascending hydrothermal fluids that brecciated the phosphorite slabs and then cemented and replaced the brecciated mega-clasts by hydrothermal Mn oxides. The enriched metals (e.g., Mn, Co, Ni, Pb, Mo, and Tl) in the nodules and stratabound layers may have been carried by these ascending fluids. The system of faults generated as a response to the Cenozoic reactivation during the Pyrenean orogeny, which

also affected Galicia Bank [*Vázquez et al*., 2008], would have provided the conduits for hydrothermal circulation that leached the basement rocks.

The Co-rich manganese nodules and diagenetic Fe-Mn replacements of phosphorite show many similarities in geochemistry and mineralogy (Table 2 and supporting information Figure S3). The Fe-Mn-oxide cements and replacements show 7 and 10Å manganates, high Mn/Fe ratios, and moderate to high Li contents, characteristics of a hydrothermal component. The high Tl or V can also be interpreted as derived from hydrothermal fluids. The difference between Fe-Mn diagenetic layers and Co-rich manganese nodules is clearly seen in the REY patterns (Figure 8). The Fe-Mn stratabound layers preserve the REY patterns characteristic of unaltered phosphorites from the Galicia Bank area, whereas Co-rich Mn nodules show significant Eu anomalies. All these parameters indicate that the Co-rich manganese nodules and Fe-Mn impregnations and replacements of phosphorites are predominantly of hydrothermal origin with a common mineralization fluid. We suggest that this difference in REY patterns can be interpreted as different products of mineralization from the same hydrothermal fluids: (a) Fe-Mn stratabound replacements of CFA by (Fe)-Mn oxyhydroxides took place by more focused flow of hydrothermal fluids through fracture and fault systems that mineralized and brecciated the hardgrounds; and (b) Co-rich manganese nodules formed in a diffuse-flow system of hydrothermal fluids within soft sediment.

5.4. Middle and Late Miocene Hydrogenetic Fe-Mn Crusts

Fe-Mn crusts cover hard rock substrates in the Galicia Bank regions as they do on many other seamounts in the global ocean [e.g., *Manheim and Lane-Bostwick*, 1988; *Koschinsky et al*., 1997; *Hein et al*., 1997; *Hein*, 2004; *Hein et al*., 2013].

5.4.1. Age Constraints of Mineralization and Contourite Drift Deposits

The Fe-Mn crusts show average thicknesses of 7–8 mm (maximum 15 mm) and high contents of Co, which indicate slow growth rates ($\sim$1.6 mm Ma^{-1} for the Fe-Mn crust in Table 2). The age of the Fe-Mn crusts is estimated to be younger than about 9.5 Ma based on the thickest crust and using the empirical equation of *Manheim and Lane-Bostwick* [1988]. This equation does not identify possible growth hiatuses during the accretion process so the calculated rates of growth are semiquantitative and represent maximum values and the calculated ages are minimum ages [*Hein et al*., 1990; *Frank et al*., 1999]. This indicates that growth of the hydrogenetic Fe-Mn crusts in the Galicia Bank region was initiated during the late Miocene, coeval with the formation of the contourite drift of seismic Unit U2 (Figure 10 and supporting information Figure S2). This giant contourite drift body migrated up slope from 1570 to 1125 m water depths over a ramp formed by the phosphatized D1 unconformity. Thus, Fe-Mn crusts grew progressively on a nondeposition surface that was not overlapped by the upslope migration of the contourite drift (supporting information Figure S2). We suggest that this contourite drift deposited along the foot and slopes of Galicia Bank was driven by vigorous south-flowing deep water bottom currents due to the introduction of Norwegian Sea Water into the North Atlantic [e.g., *de Graciansky et al*., 1984; *Stoker et al*., 2001; *Müller-Michaelis et al*., 2013]. This indicates that vigorous current activity prevented deposition of sediment and kept bare rock exposed, necessary for the growth of the crusts.

5.4.2. Paleoenvironmental Constrains and Genesis

All the Fe-Mn crusts show similar petrographic, mineralogical, and chemical compositions: thin colloform laminations of vernadite and amorphous Fe-Mn oxides, subequal amounts of Fe and Mn (Mn/Fe ratio $\sim$1), strongly positive Ce anomaly, no Eu anomaly, negative Y anomaly, and high contents of REY and trace metals (Figure 8). The chemical composition and discrimination plots clearly show a hydrogenetic origin of these thin crusts (Figure 11), which coat all hard substrates and previously mineralized rocks (Fe-Mn nodules and phosphorite slabs). Thus, either the hard substrates were relatively recently swept free of sediment or have been only intermittently exposed. We suggest that during the formation of the drift deposits of Unit U2, alternate periods of strong and weak bottom currents may have alternated giving rise to exhumation and burial stages with periods of dissolution or nongrowth alternating with periods of growth of the Fe-Mn crusts.

5.5. The Pliocene D2 Unconformity, Impingement of Mediterranean Outflow Water, and Formation of Fe-Rich Nodules

A major erosional unconformity named D2 affected the entire Galicia Bank region (supporting information Figure S2) and adjacent basin (supporting information Figure S1). This erosional unconformity produced moats around the banks and seamounts. A sequence of stepped coral mounds intercalated with contourite

drifts overlies this erosional unconformity, termed R1 by *Somoza et al*. [2014]; they correlated R1 with the RD1 erosional unconformity that occurs on Porcupine Bank [*Van Rooij et al*., 2003]. This was interpreted as a late Pliocene regional unconformity related to the reintroduction of MOW in the NE Atlantic [e.g., *Stow*, 1982]. Moreover, data from IOPD Expedition 307 at Porcupine Bank showed that coral growth started around 2.7 Ma [*Kano et al*., 2011]. Since the late Pliocene, the MOW has impinged on Galicia Bank creating initially an abrupt increase in salinity (above 35.9‰) and a marked decrease in oxygen (below 5.45 mg/L) at the seabed with respect to the adjacent Eastern North Atlantic Central Waters (ENACW).

5.5.1. Pliocene-Quaternary Fe-Rich Nodules

We suggest that this change in the oceanographic regime due to the MOW impinging on Galicia Bank caused a change in the type of seabed mineralization from Miocene to Pliocene. Moreover, along the trajectory of the MOW flow sourced from Gibraltar Strait, the type of mineralization shows the same geochemical characteristics. For example, the Fe-rich nodules and thin crusts collected from the Gulf of Cádiz along the Mediterranean undercurrent channels show similar characteristics to the Fe-rich nodules in the Galicia Bank area [*González et al*., 2012]. The Fe-rich nodules recovered at stations DRR37 and DRR38 are related to the MOW (supporting information Figures 3 and 5).

The time of Fe-rich nodule formation is constrained to seismic Unit U3, which overlies the regional erosional unconformity D2. As discussed above, we interpret this unconformity to be caused by the reintroduction of MOW in the NE Atlantic at least from 2.4 Ma.

5.5.2. Paleoenvironmental Condition and Constrains

Unit U3 is related to the MOW and developed at the summit of Galicia Bank by deep water coral mounds and intercalated with upslope migrating sediment drifts at water depths from 1125 to 826 m [*Somoza et al*., 2014]. The sedimentary cover consists of sand waves 3–7 m high and 120–150 m wavelengths. Current speed measurements yielded values ranging from 5 to 30 cm/s with average values of 8 cm/s. This environment was favorable for the diagenetic growth of Fe-rich nodules within muddy-sandy drift bodies. During glacial-interglacial cycles, alternating periods of nondeposition and/or erosion resulted from alternating strong and less vigorous bottom currents that allowed for the construction of the sedimentary drifts. These alternating periods of erosion and sedimentation likely caused variations in the redox boundary, which promoted formation of the Fe-rich nodules and their successive exhumation and burial.

5.5.3. Proposed genetic Model

The tabular Fe-rich nodules contain redox-sensitive minerals, such as pyrite (Figure 7f). The tabular form reflects mineralization fronts associated with redox boundaries in the sediment column during early diagenesis, as also occur in Fe-Mn nodules from the Gulf of Cadiz [*González et al*., 2012]. Compared to average compositional values reported from deep-sea nodules [*Baturin*, 1988], the Fe-rich nodules show very low Mn/Fe ratios (0.03–0.09) and low trace metal and REY contents (Table 2). They are enriched in Fe, Mg, As, V, and B and are quite similar to nodules collected from the Gulf of Cadiz and Black Sea [*Baturin et al*., 2002; *González et al*., 2009]. The nodules are almost pure ironstone (Mn/Fe = 0.03) end-member based on the classification of oceanic nodules using the ternary diagram Mn-Fe-(Cu + Ni + Co) × 10 [*Bonatti et al*., 1972; *Lyle*, 1981; *Dymond et al*., 1984]. Abundant references report on nodules from shallow waters and continental margins where Fe, Mn, and trace metal contents are rather similar to these Galicia Bank Fe-rich nodules [e.g., *Calvert and Price*, 1977; *Boström et al*., 1982; *Ingri*, 1985; *Glasby et al*., 1987, 1997; *Baturin et al*., 2002; *González et al*., 2007]. They all show low Mn/Fe ratios as a result of fast growth rates associated with diagenetic processes, emphasizing the importance of sediment diagenetic processes [*Reyss et al*., 1982]. This relatively rapid accretion is one of the main causes for the overall low content of transition metals in these nodules.

On bivariate diagram of Ce_{SN}/Ce_{SN^*} versus Nd concentration (Figure 11), the Fe-rich nodules lack Ce anomalies and Nd concentrations are low (5–10 μg/g). In the bivariate diagram of Ce_{SN}/Ce_{SN^*} versus Y_{SN}/Ho_{SN} ratio (Figure 11), the Fe-rich nodules show slight negative Y and Ce anomalies. Both diagrams discriminate these nodules as diagenetic in origin, but overlaps slightly with the hydrothermal field.

The high contents of B, V, and As in these nodules probably reflect contributions from hydrothermal circulation combined with the affinity of these elements for sorption by goethite. We suggest that the origin of these Fe-rich nodules might be linked to hydrocarbon-rich fluids (perhaps sourced from the underlying black shale unit) that underwent microbial degradation in the sulphate reduction-methanogenic transitional diagenetic zone and was oxidized periodically by exhumation due to vigorous MOW currents, as also proposed for the Gulf of Cádiz deposits [*González et al*., 2012].

6. Conclusions

In this paper, we analyzed for the first time a sequence of marine mineral deposits discovered on Galicia Bank (NE Atlantic Iberia margin). The mineral deposits include four types: (1) phosphorite slabs and nodules, (2) Fe-Mn crusts and stratabound deposits, (3) Co-rich Mn nodules, and (4) Fe-rich nodules. Using a combination of geophysics, mineralogy, geochemistry, and isotopic analyzes, we were able to relate the different types of mineralization to tectonic and paleoceanographic events and fluid-transport processes.

1. From the late Oligocene to early Miocene, three growth generations of phosphorites were identified within the Galicia Bank region (1) late Oligocene (~25.7–24 Ma), (2) early Miocene (23.8–22.6 Ma), and (3) latest early Miocene (18.6–16.8 Ma). The events of phosphatization occurred during transitions from glacial to warm climates in the late Oligocene-early Miocene, coincident with the phosphogenetic episodes over a wide area of the equatorial Pacific and Atlantic [*Hein et al*., 1993; *Jones et al*., 2002]. These phosphatization events indicate that moderate upwelling occurred also in the NE Atlantic during those periods of transition.
2. During the late Oligocene to latest early Miocene, the progressive decrease in ε_{Nd} values for the phosphatization events is interpreted to reflect increasing influence of the Northern Component Water (NCW) caused by the progressive opening of the northern gateways [e.g., *Müller-Michaelis et al*., 2013].
3. During the latest early Miocene, hydraulic fracturing of the phosphorite hardground was caused by regional intraplate tectonism in the North Atlantic, forming a widespread North Atlantic erosional unconformity (~19–17 Ma), termed D1. This regional unconformity occurring in the deep North Atlantic is associated with activity of the Iceland hot spot and opening of the Iceland-Faroe Channel and Rockall Trough. In the Galicia Bank region, the North Atlantic tectonism was transferred as compressional stress promoting subduction of the northern Biscay Bay oceanic crust beneath the continental crust of the North Iberian margin.
4. During this latest early Miocene episode of active tectonism, Mn-impregnations of the phosphorite hardgrounds formed stratabound layers, and Co-rich manganese nodules with remarkably high Co contents (to 1.8 wt %) and other trace metals, and with significant Eu anomalies. These deposits are interpreted to have been derived from metal-rich hydrothermal fluids that leached organic-matter-rich sediments and/or continent basement rocks underlying the bank and adjacent seamounts. Seismic-delineated chimneys reflect ascending fluids and sediments (diapirs) in the vicinity of hydrofractured metalliferous phosphorites and Co-rich nodules. Reactivated faults were the main fluid transport pathways and high geothermal gradients associated with thinned crust drove the hydrothermal circulation cells.
5. During the middle and late Miocene, and once the Scotland-Iceland gateways opened, the introduction of vigorous deep-sourced water from the Arctic impinged directly on Galicia Bank through Rockall Trough. This deep water flow promoted precipitation of hydrogenetic Fe-Mn crusts enriched in Co and Ce by keeping substrate rock free of sediment accumulation. The Fe-Mn crusts are estimated to have started growth around 9.5 Ma ago.
6. During the late Pliocene, the growth of diagenetic Fe-rich nodules with low contents of Mn and trace metals was associated with the reintroduction of hypersaline Mediterranean Outflow Water by opening of the Africa-Europe gateway at about 2.4 Ma. Moreover, along the trajectory of the MOW, sourced from Gibraltar Strait, mineralization shows the same geochemical characteristics. Thus, the Fe-rich nodules and crusts collected from the Gulf of Cádiz along the Mediterranean undercurrent channels show similar characteristics as the Galicia Bank area Fe-rich nodules [*González et al*., 2012].

We interpret this succession of mineralization as controlled by major changes in the oceanographic and tectonic regimes that triggered the present global thermohaline circulation (THC) during the Cenozoic through the introduction of Arctic and Mediterranean waters into the North Atlantic Ocean. Traditionally, the Eocene/Oligocene boundary at about 33.9 Myr ago marks the transition from a greenhouse to icehouse world [e.g., *Abelson et al*., 2008]. We conclude based on data for the mineral deposits from Galicia Bank that the transition between the greenhouse phosphorite mineralization and icehouse Fe-Mn crust mineralization, that occurred after the last event of phosphatization, took place during the latest early Miocene (~18.6–16.8 Ma). This marked change in the type of mineralization on Galicia Bank is coeval with a widespread regional unconformity (19–17 Ma) identified in the North Atlantic deep basins linked to the opening of the gateway for Arctic-sourced deep water flow into the North Atlantic [e.g., *Dingle et al*., 1982; *Stoker*

et al., 2001; *Müller–Michaelis et al*., 2013]. Furthermore, a major intraplate tectonic event occurred in the NE Atlantic during this period, the suppression of the Iceland hot spot plume and/or the rifting of Rockall Trough seem to have played an important role in triggering rapid deepening of the Greenland-Scotland Ridge, the sill between the Nordic Seas and North Atlantic. We suggest that this major oceanographic/tectonic event promoted the hydrofracturing of the phosphorite hardground and the subsequent Mn replacement of the margins of phosphorite slabs as well as formation of the striking Co enrichment of the manganese nodules associated with hydrothermal fluids. These types of mineral deposits are testimony of the abrupt climate transition between a greenhouse and icehouse world and by regional intraplate tectonics that opened the passage of Nordic waters into the Atlantic and triggered the present global thermohaline circulation.

Acknowledgments

This work has been supported by the Spanish projects DIVA-ARTABRIA II (PGIDIT07PXB000120PR), CONTOUR-IBER (CTM 2008-06399-C04/MAR), ERGAP (VEM 2003-20093-CO3), and SUBVENT (CGL2012-39524-C02) and the European project EMODnet-Geology (2012/S96-158476). The authors thank all the scientific and technical staff who participated in the oceanographic cruises of the DIVA-ARTABRIA and ERGAP projects onboard the *R/V Sarmiento de Gamboa* and *R/V LAtalante* for data acquisition and for their expertise in collecting the samples. We also thank the staff of the "Estación de Bioloxía Mariña da Graña" at the Santiago de Compostela University (USC), "National Center of Electronic Microscopy," "Center of Geochronology and Isotopic Geochemistry" at the Complutense University of Madrid (UCM), Laboratories of the "Pacific Coastal and Marine Science Center" (USGS), and the Laboratories of the "Geological Survey of Spain" (IGME) for allowing us to use their facilities. Jorge Civis and Luis Granados are grateful for their help in micropaleontological identifications. The geophysical data and samples necessary to produce this paper are available from the authors upon request (fj.gonzalez@igme.es). The materials are archived at the Geological Survey of Spain (IGME). We thank G. Filippelli and four anonimous reviews and Editors for comments that helped improve this paper.

References

Abelson, M., A. Agnon, A. Almogi-Labin (2008), Indications for control of the Iceland plume on the Eocene-Oligocene ''greenhouse-icehouse'' climate transition. *Earth Plan. Sci. Lett.*, *265*, 33–48.

Alvarez-Marrón, J., E. Rubio, and M. Torne (1997), Subduction related structure in the North Iberian Margin, *J. Geophys. Res.*, *102*(B10), 22,497–22,511.

Ambar, I., and M. R. Howe (1979), Observations of the Mediterranean outflow. 2. Deep circulation in the vicinity of the Gulf of Cadiz, *Deep Sea Res., Part A*, *26*(5), 555–568.

Aplin, A. C., and D. S. Cronan (1985), Ferromanganese oxide deposits from the Central Pacific Ocean, I. Encrustations from the Line Island archipelago, *Geochim. Cosmochim. Acta*, *49*, 427–436.

Arning, E. T., D. Birgel, H. N. Schulz-Vogt, L. Holmkvist, B. B. Jørgensen, A. Larsson, and J. Peckmann (2008), Lipid biomarker patterns of phosphogenic sediments from upwelling regions, *Geomicrobiol. J.*, *25*, 69–82.

Arning, E. T., A. Lückge, C. Breuer, N. Gussone, D. Birgel, and J. Peckmann (2009), Genesis of phosphorite crusts off Peru, *Mar. Geol.*, *262*, 68–81.

Baturin, G. N. (1982), *Phosphorites on the Sea Floor*, 343 pp., Elsevier, Amsterdam.

Baturin, G. N. (1988), *The Geochemistry of Manganese and Manganese Nodules in the Ocean*, 342 pp., D. Riedel Publ. Co., Berlin.

Baturin, G. N., and I. G. Drovetsova (2014), Hydrothermal manganese mineralization in the Peterbourgskoye Ore Field (North Atlantic), *Oceanology*, *54-2*, 222–230.

Baturin, G. N., and V. T. Dubinchuk (2011), Mineralogy and chemistry of ferromanganese crusts from the Atlantic Ocean, *Geochem. Int.*, *49*, 578–593.

Baturin, G. N., A. I. Gorshkov, L. O. Magazina, and O. Yu. Bogdanova (2002), Structure and composition of ferromanganese-phosphate nodules from the Black Sea, *Lithol. Miner. Res.*, *37*, 374–385.

Bau, M., K. Schmidt, A. Koschinsky, J. Hein, T. Kuhn, and A. Usui (2014), Discriminating between different genetic types of marine ferromanganese crusts and nodules based on rare earth elements and yttrium, *Chem. Geol.*, *381*, 1–9.

Bau, M., A. Koschinsky, P. Dulski, J. R. Hein (1996), Comparison of the partitioning behaivours of yttrium, rare-earth elements, and titanium between hydrogenetic marine ferromanganese crusts and seawater, *Geochim. Cosmochim. Acta*, *60*, 1709–1725.

Benninger, L. M., and J. R. Hein (2000), Diagenetic evolution of seamount phosphorite, in *Marine Authigenesis: From Global to Microbial*, edited by C. R. Glenn, L. Prévôt-Lucas, and J. Lucas, *Spec. Publ. SEPM Soc. Sediment. Geol.*, 66, 245–256.

Bentor, Y. K. (1980), Marine phosphorites-geochemistry, occurrence, genesis, Spec. Publ. Soc. Econ. Paleontol. Mineral., 29, 249 pp.

Birch, G. F. (1980), A model of penecontempoaneous phosphatization by diagenetic and authigenic mechanism from the western margin of southern Africa, in *Marine Phosphorites—Geochemistry, Occurrence, Genesis*, edited by Y. K. Bentor, Spec. Publ. Soc. Econ. Paleontol. Mineral., 29, 79–100.

Black, M. (1964), Cretaceous and Tertiary coccoliths from Atlantic seamounts, *Paleontology*, *7-2*, 306–316.

Bode, A., M. Varela, B. Casas, and N. González (2002), Intrusions of eastern North Atlantic central waters and phytoplankton in the north and northwestern Iberian shelf during spring, *J. Mar. Syst.*, *36*, 197–218.

Boillot, G., and J. Malod (1988), The north and north-west Spanish continental margin: A review, *Rev. Soc. Geol. Esp.*, *1*, 295–316

Bonatti, E., T. Kraemer, and H. Rydell (1972), Classification and genesis of submarine iron-manganese deposits, in *Ferromanganese Deposits of the Ocean Floor*, edited by D. R. Horn, pp. 149–165, Arden House, N. Y.

Boström, K., L. Wiborg, and J. Ingri (1982), Geochemistry and origin of ferromanganese concretions in the Gulf of Bothnia, *Mar. Geol.*, *50*, 1–24.

Burnett, W. C. (1977), Geochemistry and origin of phosphorite deposits from off Peru and Chile, *Geol. Soc. Am. Bull.*, *88*, 813–823.

Burnett, W. C., and S. R. Riggs (1990), *Phosphate Deposits of the World, vol. 3, Neogene to Modern Phosphorites*, Cambridge Univ. Press, Cambridge.

Calvert, S. E., and N. B. Price (1977), Shallow water, continental margin and lacustrine nodules: Distribution and geochemistry, in *Marine Manganese Deposits, Elsevier Oceanogr. Ser.*, edited by G. P. Glasby, pp. 45–86, Elsevier, Amsterdam.

Capdevila, R., and D. Mougenot (1988), The pre-mesozoic basement of the western Iberian continental margin and its place in the Variscan belt, in *Proceedings of the Ocean Drilling Program, Scientific Results*, vol. 103, edited by G. Boillot et al., pp. 3–12, U.S. Gov. Print. Off., Washington, D. C.

Daniault, N., J. M. Mazem, and M. Arhan (1994), Circulation and mixing of Mediterranean water west of the Iberian Peninsula, *Deep Sea Res., Part I*, *41*, 1685–1714.

DeBaar, H. J. W., M. P. Bacon, P. G. Brewer, and K. W. Bruland (1985), Rare-earth elements in the Pacific and Atlantic Oceans, *Geochim. Cosmochim. Acta*, *49*(9), 1943–1959.

De Carlo, E. H., P. A. Pennywell, and C. M. Fraley (1987), Geochemistry of ferromanganese deposits from the Kiribati and Tuvalu region of the west central Pacific Ocean, *Mar. Min.*, *6*, 301–321.

de Graciansky, P. C., et al. (1984), Site 548, *Initial Rep. Deep Sea Drill. Proj.*, *80*, 33–122.

Dingle, R. V., J. B. Megson, and R. A. Scrutton (1982), Acoustic stratigraphy of the sedimentary succession west of Porcupine Bank, N.E. Atlantic Ocean: A preliminary account, *Mar. Geol.*, *47*, 17–35.

Dupeuble, P. A., J. P. Rehault, J. L. Auxietre, J. P. Dunand, and L. Pastouret (1976), Results of Dredgings and Stratigraphy of Galicia Bank, and Vigo and Porto Seamounts (Iberic Continental-Margin), *Mar. Geol.*, *22*(2), M37–M49.

Dymond, J., M. Lyle, B. Finney, D. Z. Piper, K. Murphy, R. Conard, and N. Pisias (1984), Ferromanganese nodules from MANOP Sites H, S and R- control of mineralogical and chemical composition by multiple accretionary processes, *Geochim. Cosmochim. Acta*, *48*, 931–950.
Ercilla, G., D. Casas, L. Somoza, J. T. Vázquez, J. Iglesias, S. García-Gil, T. Medialdea, R. León, F. Estrada, and ERGAP Project and Cruise Teams (2009), Cartografiando la dinámica sedimentaria dela región del Banco de Galicia, in *6° Simposio Sobre el Márgen Ibérico Atlántico*, pp. 201–204, ASG, Oviedo.
Ercilla, G., et al. (2011), Imaging the recent sediment dynamics of the Galicia Bank region (Atlantic, NW Iberian Peninsula), *Mar. Geophys. Res.*, *32 I*(1-2), 99–126.
Filippelli, G. M. (2011), Phosphate rock formation and marine phosphorus geochemistry: The deep time perspective, *Chemosphere*, *84*, 759–766.
Fiúza, A. F. G. (1984), Hidrologia e dinâmica das aguas costeiras de Portugal, PhD thesis, 294 pp., Univ. de Lisboa, Lisboa.
Follmi, K. B. (1990), Condensation and phosphogenesis: Example of the Helvetic mid-Cretaceous (northern Tethyan margin), in *Phosphorite Research and Development*, edited by A. *J. G. Notholt and I. Jarvis, Geol. Soc. Spec. Publ.*, *52*, 237–252.
Föllmi, K. B. (1996), The phosphorus cycle, phosphogenesis and marine phosphate-rich deposits, *Earth Sci. Rev.*, *40*, 55–124.
Flower, B. P., and J. P. Kennet (1993), Middle Miocene ocean climate transition: High-resolution oxygen and carbon isotopic records from Deep Sea Drilling Project Site 588A, Southwest Pacific, *Paleoceanography*, *8*(6), 811–843.
Frank, M., R. K. O'Nions, J. R. Hein, and V. K. Banakar (1999), 60 Myr records of major elements and Pb-Nd isotopes from hydrogenous ferromanganese crusts: Reconstruction of seawater paleochemistry, *Geochim. Cosmochim. Acta*, *63*, 1689–1708.
Froelich, P. N., et al. (1988), Early diagenesis of organic-matter in Peru continental-margin sediments-phosphorite precipitation, *Mar. Geol.*, *80*, 309–343.
Garcia-Lafuente, J., J. C. Sánchez-Garrido, G. Díaz del Rio, F. Criado Aldeanuela, D. Marcote, and A. Sánchez Román (2008), Low-frequency variability of the Mediterranean undercurrent off Galicia, northwestern Iberian Peninsula, *J. Mar. Syst.*, *74*, 351–363.
GEBCO (2003), *IOC, IHO and BODC, Centenary Edition of the GEBCO Digital Atlas [CD-ROM]*, Br. Oceanogr. Data Cent., Liverpool, U. K.
Glasby, G. P., R. Gwozoz, H. kunzendorf, G. Friedrich, and T. Thijssen (1987), The distribution of rare earth and minor elements in manganese nodules and sediments for the equator and SW Pacific, *Lithos*, *20*, 97–113.
Glasby, G. P., E. M. Emelyanov, V. A. Zhamoida, G. N. Baturin, T. Leipe, R. Bahlo, and P. Bonacker (1997), Environments of formation of ferromanganese concretions in the Baltic Sea: A critical review, in *Manganese Mineralization: Geochemistry and Mineralogy of Terrestrial and Marine Deposits*, edited by K. Nicholson et al., Geol. Soc. Spec. Publ., 119, 213–237.
Glenn, C. R., and M. A. Arthur (1988), Petrology and major element geochemistry of Peru margin phosphorites and associated diagenetic minerals: Authigenesis in modern organic-rich sediments, *Mar. Geol.*, *80*, 231–267.
González, F. J., L. Somoza, R. Lunar, J. Martínez-Frías, J. A. Martín Rubí, T. Torres, J. E. Ortiz, and V. Díaz del Río (2007), Fe-Mn nodules associated with hydrocarbon seeps: A new discovery in the Gulf of Cadiz (eastern Central Atlantic), *Episodes*, *30*(3), 187–196.
González, F. J., L. Somoza, R. Lunar, J. Martínez-Frías, J. A. Martín Rubí, T. Torres, J. E. Ortiz, V. Díaz del Río, L. M. Pinheiro, and V. H. Magalhães (2009), Hydrocarbon-derived ferromanganese nodules in carbonate-mud mounds from the Gulf of Cadiz: Mud breccia sediments and clasts as nucleation sites, *Mar. Geol.*, *261*, 64–81.
González, F. J., L. Somoza, R. León, T. Medialdea, T. Torres, J. E. Ortiz, R. Lunar, J. Martínez-Frías, and R. Merinero (2012), Ferromanganese nodules and micro-hardgrounds associated with the Cadiz Contourite Channel (NE Atlantic): Palaeoenvironmental records of fluid venting and bottom currents, *Chem. Geol.*, *310-311*, 56–78.
Groupe Galicia (1979), The continental margin off Galicia and Portugal: Acoustical stratigraphy, dredge stratigraphy and structural evolution, in *Initial Report of the Deep Sea Drilling Project*, vol. 47, edited by Sibuet et al., pp. 633–662, U.S. Gov. Print. Off., Washington, D. C.
Harvey, J. (1982), Θ–S relationship and water masses in the eastern North Atlantic, *Deep Sea Res., Part A*, *95*, 11,425–11,441.
Hein, J. R. (2004), Cobalt-rich ferromanganese crusts: Global distribution, composition, origin and research activities, in *Proceedings of the Workshop on Minerals Other than Polymetallic Nodules of the International Seabed Area*, vol. 1, pp. 188–256, Int. Seabed Auth., Kingston.
Hein, J. R., and A. Koschinsky (2014), Deep-ocean ferromanganese crusts and nodules, in *Treatise on Geochemistry*, vol. 13, 2nd ed., edited by H. D. Holland and K. K. Turekian, chap. 11, pp. 273–291, Elsevier, Oxford, U. K., doi:10.1016/B978-0-08-095975-7.01111-6.
Hein, J. R., and C. L. Morgan (1999), Influence of Substrate rocks on Fe-Mn Crust Composition, *Deep Sea Res., Part I*, *46*, 855–875.
Hein, J. R., F. T. Manheim, W. C. Schwab, and A. S. Davis (1985), Ferromanganese crusts from Necker Ridge, Horizon Guyot, and S.P. Lee Guyot: Geological considerations, *Mar. Geol.*, *69*(1/2), 25–54.
Hein, J. R., M. S. Schulz, and J.-K. Kang (1990), Insular and submarine ferromanganese mineralization of the Tonga-Lau region, *Mar. Min.*, *9*(3), 305–354.
Hein, J. R., H.-W. Yeh, S. H. Gunn, W. V. Sliter, L. M. Benninger, and C.-H. Wang (1993), Two major Cenozoic episodes of phosphogenesis recorded in equatorial Pacific seamount deposits, *Paleoceanography*, *8*(2), 293–311.
Hein, J. R., A. Koschinsky, P. Halbach, F. T. Manheim, M. Bau, J.-K. Kang, and N. Lubick (1997), Iron and manganese oxide mineralization in the Pacific, in *Manganese Mineralization: Geochemistry and Mineralogy of Terrestrial and Marine Deposits*, edited by K. Nicholson et al., *Geol. Soc. Spec. Publ.*, *119*, 123–138.
Hein, J. R., A. Koschinsky, M. Bau, F. T. Manheim, J.-K. Kang, and L. Roberts (2000), Cobalt-rich ferromanganese crusts in the Pacific, in *Handbook of Marine Mineral Deposits*, edited by D. S. Cronan, pp. 239–279, CRC Press, Boca Raton, Fla.
Hein, J. R., A. Koschinsky, and B. R. McIntyre (2005), Mercury- and silver-rich ferromanganese-oxides, Southern California Borderland: Deposit model and environmental implications, *Econ. Geol.*, *100*(6), 1151–1168.
Hein, J. R., T. A. Conrad, and H. Staudigel (2010), Seamount mineral deposits, a source of rare-metals for high technology industries, *Oceanography*, *23*(1), 184–189.
Hein, J. R., K. Mizell, A. Koschinsky, and T. A. Conrad (2013), Deep-ocean mineral deposits as a source of critical metals for high- and green-technology applications: Comparison with land-based deposits, *Ore Geol. Rev.*, *51*, 1–14.
Hein, J. R., F. Spinardi, N. Okamoto, K. Mizell, D. Thorburn, and A. Tawake (2015), Critical metals in manganese nodules from the Cook Islands EEZ, abundances and distributions, *Ore Geol. Rev.*, *68*, 97–116.
Ingri, J. (1985), Geochemistry of ferromanganese concretions and associated sediments in the Gulf of Bothnia, PhD thesis, Univ. of Lulea, Lulea, Sweden.
Iorga, M., and M. S. Lozier (1999), Signatures of the Mediterranean outflow from a North Atlantic climatology: 1. Salinity and density fields, *J. Geophys. Res.*, *104*(C11), 25,985–26,009.
Jarvis, I. (1992), Sedimentology, geochemistry and origin of phosphatic chalks: The Upper Cretaceous deposits of NW Europe, *Sedimentology*, *39*, 55–97.
Jones, E. J. W., M. K. BouDagher-Fadel, and M. F. Thirlwall (2002), An investigation of seamount phosphorites in the Eastern Equatorial Atlantic, *Mar. Geol.*, *183*(1-4), 143–162.

Kano, A., et al. (2011), Age constraints on the origin and growth history of a deep-water coral mound in the northeast Atlantic drilled during Integrated Ocean Drilling Program Expedition 307, *Geology*, *35*, 1051–1054.
Koschinsky, A., and J. R. Hein (2003), Uptake of elements from seawater by ferromanganese crusts: Solid phase association and seawater speciation, *Mar. Geol.*, *98*, 331–351.
Koschinsky, A., A. Stascheit, M. Bau, and P. Halbach (1997), Effects of phosphatization on the geochemical and mineralogical composition of marine ferromanganese crusts, *Geochim. Cosmochim. Acta*, *61*, 4079–4094.
Lamboy, M. (1993), Phosphatization of calcium carbonate in phosphorites: Microstructure and importance, *Sedimentology*, *40*, 53–62.
Lyle, M. (1981), Formation and growth of ferromanganese oxides on the Nazca plate, in *Nazca Plate: Crustal Formation and Andean Convergence*, edited by L. D. Kulm et al., *Geol. Soc. Am. Mem., 154*, 269–293.
Manheim, F. T., and R. A. Gulbrandsen (1979), Marine phosphorites, in *Marine Minerals, Short Course Notes*, vol. 6, edited by R. G. Burns, pp. 151–173, Mineral. Soc. of Am., Wash.
Manheim, F. T., and C. M. Lane-Bostwick (1988), Cobalt in ferromanganese crusts as a monitor of hydrothermal discharge on the Pacific sea floor, *Nature*, *335*, 59–62.
Manheim, F. T., R. M. Pratt, and P. F. McFarlin (1980), Composition and origin of phosphorite deposits of the Blake Plateau, in *Marine Phosphorites-Geochemistry, Occurrence, Genesis*, edited by Y. K. Bentor, *Spec. Publ. Soc. Econ. Paleontol. Mineral.*, 29, 117–137.
McArthur, J. M., and R. J. Howarth (2004), Sr-isotope stratigraphy: The Phanerozoic 87Sr/86Srcurve and explanatory notes, in *A Geological Timescale*, edited by F. M. Gradstein, J. G. Ogg, and A. G. Smith, pp. 96–105, Cambridge Univ. Press, Cambridge, U. K.
McCartney, M. S., and L. D. Talley (1982), The subpolar mode water of the North Atlantic Ocean, *J. Phys. Oceanogr.*, *12*, 1169–1188.
McClellan, G. H., and S. J. Van Kauwenbergh (1990), Mineralogy of sedimentary apatites, in *Phosphorite Research and Development*, edited by A. J. G. Notholt and I. Jarvis, *Geol. Soc. Spec. Publ.*, *52*, 23–31.
Müller-Michaelis, A., G. Uenzelmann-Neben, and R. Stein (2013), A revised Early Miocene age for the instigation of the Eirik Drift, offshore southern Greenland: Evidence from high-resolution seismic reflection data, *Mar. Geol.*, *340*, 1–15.
O'Brien, G., and D. Heggie (1988), *East Australian Continental Margin phosphorites, Eos Trans. AGU*, *69*, 2–2,°doi:10.1029/88EO00007.
O'Brien, G. W., A. R. Milnes, H. H. Veeh, D. T. Heggie, S. R. Riggs, D. J. Cullen, J. F. Marshall, and P. J. Cook (1990), Sedimentation dynamics and redox iron-cycling: Controlling factors for the apatite-glauconite association on the east Australian continental margin, in *Phosphorite Research and Development*, edited by A. J. G. Notholt and I. Jarvis, *Geol. Soc. Spec. Publ.*, *52*, 61–86.
Paillet, J., and H. Mercier (1997), An inverse model of the eastern North Atlantic general circulation and thermocline ventilation, *Deep Sea Res., Part I*, *44*, 1293–1328.
Palmer, M. R., and H. Elderfield (1985a), Variations in the Nd isotopic composition of foraminifera from Atlantic oceanic sediments, *Earth Planet. Sci. Lett.*, *73*, 299–305.
Palmer, M. R., and H. Elderfield (1985b), Sr isotope composition of seawater over the past 75 Myr, *Nature*, *314*, 526–528.
Pascal, M., G. Sustrac, F. Barthelemy, M. Dieng, B. Faye, C. Faye, S. Kande, and M. Seck (1989), Phosphate deposits of Senegal, in *Phosphate Deposits of the World, vol. 2, Phosphate Rock Resources*, edited by A. J. G. Notholt, R. P. Sheldon, and D. F. Davidson, pp. 233–246, Cambridge Univ. Press, Cambridge, U. K.
Pichocki, C., and M. Hoffert (1987), Characteristics of Co-rich ferromanganese nodules and crusts sampled in French Polynesia, *Mar. Geol.*, *77*, 109–119.
Piper, D. Z. (1974a), Rare earth elements in the sedimentary cycle: A summary, *Chem. Geol.*, *14*, 285–304.
Piper, D. Z. (1974b), Rare earth elements in ferromanganese nodules and other marine phases, *Geochim. Cosmochim. Acta*, *38*, 1007–1022.
Pollard, R. T., and S. Pu (1985), Structure and circulation of the upper Atlantic Ocean northeast of the Azores, *Prog. Oceanogr.*, *14*, 443–462.
Price, N. B., and S. E. Calvert (1978), The geochemistry of phosphorites from the Namibian Shelf, *Chem. Geol.*, *23*, 151–170.
Rao, V. P., and W. C. Burnett (1992), Phosphatic rocks and manganese crusts from seamounts in the EEZ of Kiribati and Tuvalu, central Pacific Ocean, in *Geology and Offshore Mineral Resources of the Central Pacific Basin*, edited by B. H. Keating and B. R. Bolton, pp. 285–296, Springer, N. Y.
Reyss, J. L., V. Marchig, and T. L. Ku (1982), Rapid growth of a deep-sea manganese nodule, *Nature*, *295*, 401–403.
Rios, A. F., F. F. Pérez, and F. F. Fraga (1992), Water masses in the upper and middle North Atlantic Ocean east of the Azores, *Deep Sea Res., Part A*, *39*, 645–658.
Rodríguez Fernández, L. R., et al. (2016), Mapa Geológico de España y Portugal a escala 1:1.000.000, Margen Continental, Inst. Geol. y Minero de España, Madrid, in press.
Rona, P. A. (2008), The changing vision of marine minerals, *Ore Geol. Rev.*, *33*, 618–666.
Saunders, P. M. (1986), The accuracy of measurement of salinity, oxygen and temperature in the deep ocean, *J. Phys. Oceanogr.*, *16*, 189–195.
Schulz, H. N., and H. D. Schulz (2005), Large sulfur bacteria and the formation of phosphorite, *Science*, *307*, 416–418.
Somoza, L., G. Ercilla, V. Urgorri, R. León, T. Medialdea, M. Paredes, F. J. González, and M. A. Nombela (2014), Detection and mapping of cold-water coral mounds and living Lophelia reefs in the Galicia Bank, Atlantic NW Iberia margin, *Mar. Geol.*, *349*, 73–90.
Stille, P., M. Steinmann, and S. R. Riggs (1996), Nd isotope evidence for the evolution of the paleocurrents in the Atlantic and Tethys Oceans during the past 180 Ma, *Earth Planet. Sci. Lett.*, *144*, 9–19.
Stoker, M. S., T. C. E. van Weering, and T. Svaerdborg (2001), A mid- to late Cenozoic tectostratigraphic framework for the Rockall Trough, in *The Petroleum Exploration of Ireland's Offshore Basins*, edited by P. M. Shannon, P. Haughton, and D. Corcoran, *Geol. Soc. Spec. Publ.*, *188*, 411–438.
Stoker, M. S., D. Long, and J. Bulat (2002), A record of Mid-Cenozoic deep-water erosion in the Faroe Shetland Channel, in *European Margin Sediment Dynamics—Sidescan Sonar and Seismic Images*, edited by J. Mienert and P. Weaver, pp. 145–148, Springer, Berlin.
Stoker, M. S., R. J. Hoult, T. Nielsen, B. O. Hjelstuen, J. S. Laberg, P. M. Shannon, D. Praeg, A. Mathiesen, T. C. E. van Weering, and A. McDonnell (2005), Sedimentary and oceanographic responses to early Neogene compression on the NW European margin, *Mar. Pet. Geol.*, *22*, 1031–1044.
Stow, D. A. V. (1982), Bottom currents and contourites in the North Atlantic, *Bull. Inst. Geol. Bassin Aquitaine*, *31*, 151–166.
Tooms, J. S., and C. P. Summerhayes (1968), Phosphatic rocks from the northwest African continental shelf, *Nature*, *218*, 1241–1242.
Turekian, K. K., and K. H. Wedepohl (1961), Distribution of the Elements in some major units of the Earth's crust, *Geol. Soc. Am. Bull.*, *72*, 175–192.
Usui, A., and M. Someya (1997), Marine Mn deposits in NW Pacific, in *Manganese Mineralization: Geochemistry and Mineralogy of Terrestrial and Marine Deposits*, K. Nicholson et al., Spec. Publ. Geol. Soc., *119*, 177–198.
Van Aken, H. M. (2000), The hydrography of the mid-latitude Northeast Atlantic Ocean II: The intermediate water masses, *Deep Sea Res., Part I*, *47*, 789–824.

Vanney, J. R., J. L. Auxiètre, and J. P. Dunand (1979), Geomorphic provinces and the evolution of the northwestern Iberian Continental Margin, *Ann. Inst. Oceanogr. Paris*, *55*(1), 5–20.

Van Rooij, D., B. De Mol, V. Huvenne, M. K. Ivanov, and J. P. Henriet (2003), Seismic evidence of current-controlled sedimentation in the Belgica mound province, upper Porcupine slope, southwest of Ireland, *Mar. Geol.*, *195*(1–4), 31–53.

Vázquez, J. T., T. Medialdea, G. Ercilla, L. Somoza, F. Estrada, M. C. Fernández-Puga, J. Gallart, E. Gràcia, A. Maestro, and M. Sayago (2008), Cenozoic deformational structures on the Galicia Bank Region (NW Iberian continental margin), *Mar. Geol.*, *249*(1–2), 128–149.

Vázquez, J. T., G. Ercilla, T. Medialdea, L. Somoza, F. Bohoyo, F. Estrada, and R. León (2009a), Deformaciones neotectónicas en la Zona Transicional de la región del Banco de Galicia, in *Nuevas Contribuciones al Margen Ibérico Atlántico*, edited by G. Flor Rodríguez et al., pp. 45–48, Arias Servicios Gráficos 2003 S.L., Oviedo, Spain.

Vázquez, J. T., G. Ercilla, T. Medialdea, L. Somoza, F. Bohoyo, D. Casas, F. Estrada, M. Farrán, S. García-Gil, and R. León (2009b), El colapso BURATO ERGAP: Un rasgo morfo-tectónico de primera magnitud en el Banco de Galicia, in *Nuevas Contribuciones al Margen Ibérico Atlántico*, edited by G. Flor Rodríguez et al., pp. 205–208, Arias Servicios Gráficos 2003 S.L., Oviedo, Spain.

Vincent, E., and W. H. Berger (1985), Carbon dioxide and polar cooling in the Miocene: The Monterey hypothesis, in *The Carbon Cycle and Atmospheric CO2, Natural Variations Archean to Present, Geophys. Monogr. Ser.*, pp. 455–468, AGU, Washington, D. C.

Vine, J. D., and E. B. Tourtelot (1970), Geochemistry of black shale deposits—A summary report, *Econ. Geol.*, *65*, 253–272.